Temperature Dependent Magnetic Properties of Silica Coated Maghemite Nanoparticles

By:

Shahid Iqbal
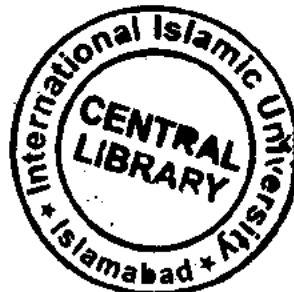(149-FBAS/MSPHY/S13)

Supervisor:

Dr. Kashif Nadeem

Assistant Professor

Department of Physics, FBAS, IIUI

Department of Physics

Faculty of Basic and Applied Sciences

International Islamic University, Islamabad

(2015)

... ...ic properies

... ...ization .

Temperature Dependent Magnetic Properties of Silica Coated Maghemite Nanoparticles

By:

Shahid Iqbal
(149-FBAS/MSPHY/S13)

Supervisor:
Dr. Kashif Nadeem
Assistant Professor

Department of Physics, FBAS, IIUI

Department of Physics

Faculty of Basic and Applied Sciences

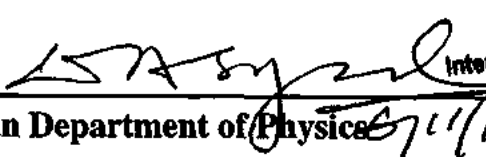## International Islamic University, Islamabad

(2015)

Temperature Dependent Magnetic Properties of Silica Coated Maghemite Nanoparticles

By:

Shahid Iqbal
(149-FBAS/MSPHY/S13)

This Thesis submitted to Department of Physics International Islamic University, Islamabad for the award of degree of MS Physics.

CHAIRMAN
DEPT. OF PHYSICS
International Islamic University
Islamabad

Chairman Department of Physics

International Islamic University Islamabad

Dean Faculty of Basic and Applied Science
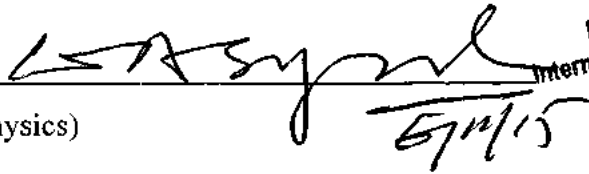International Islamic University, Islamabad

II

Final Approval

It is certified that the work presented in this thesis entitled **"Temperature Dependent Magnetic Properties of Silica Coated Maghemite Nanoparticles"** by **Shahid Iqbal,** Registration No.149-FBAS/MSPHY/S13 fulfills the requirement for the award of degree of MS Physics from Department of Physics, International Islamic University, Islamabad, Pakistan.
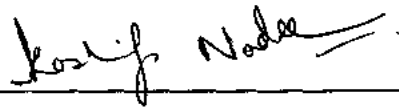
Viva Voce Committee

Chairman:

(Department of Physics)
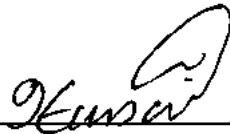
CHAIRMAN
DEPT. OF PHYSICS
International Islamic University
Islamabad

Supervisor:

External Examiner:

Internal Examiner:

بِسْمِ اللَّهِ الرَّحْمَٰنِ الرَّحِيمِ

DEDICATED

to

ALLAH (SWT)

Declaration

I, **Shahid Iqbal** (Registration # 149-FBAS/MSPHY/S13), student of MS Physics (Session 2013-2015), hereby declare that the work presented in the thesis entitled **"Temperature Dependent Magnetic Properties of Silica Coated Maghemite Nanoparticles"** in partial fulfillment of MS degree in Physics from International Islamic University Islamabad, is my own work and has not been published or submitted as research work or thesis in any form in any other university or institute in Pakistan or aboard.

Shahid Iqbal

(149-FBAS/MSPHY/S13)

Dated: _____

Forwarding Sheet by Research Supervisor

The thesis entitled "**Temperature Dependent Magnetic Properties of Silica Coated Maghemite Nanoparticles**" submitted by Shahid Iqbal (Registration # 149-FBAS/MSPHY/S13) in partial fulfillment of MS degree in Physics has been completed under my guidance and supervision. I am satisfied with the quality of his research work and allow him to submit this thesis for further process to graduate with Master of Science degree from Department of Physics, as per IIUI Islamabad rules and regulations.

Dr. Kashif Nadeem

Assistant Professor (TTS)

Department of Physics,

International Islamic University,

Islamabad.

Dated: 03/11/15

VII

Acknowledgment

Praise is to Allah Almighty who gave me strength and inspiration to complete this research project. I would like to acknowledge the worth mentioning supervision of **Dr. Kashif Nadeem** who guided me and supported me during my whole research work. Moreover, their supervision enabled me to develop an understanding of the field. Without their sincere efforts I was unable to complete this hard task of my life. Really I am thankful to **Dr. Kashif Nadeem** for their inspiration and encouragement in every field of life especially in education and teaching. Almighty Allah may bless them with long life, health, happiness and knowledge.

Moreover, I would like to express my sincere thanks to all the faculty members of Department of Physics IIU Islamabad especially to **Dr. Muhammad Mumtaz** and **Dr. Syed Salman Hussain**. I would also like to thank all other faculty members of university for their sincere appreciation, comments and suggestions. I express my thanks to all staff of Physics Department IIUI, for their various services. I shall express my heartiest thanks to all my senior research colleagues **Irfan Qasim, Waqi-Ur-Rehman, Abdul Jabbar Bhutta, Liaqat Ali, Adnan Razzaq Qureshi, Faisal Zeb** and especially to **Ghullam Hussain** for being very co-operative throughout my research work. I also pay special thanks to my class fellows **Syed Kamran Ali Shah, Muhammad Waqas** and especially to **Irfan Ali** without their guidance it was not possible to complete my work.

I especially want to acknowledge efforts and prayers of parents, brothers, and sisters and Friends. Allah may bless my parents, family and friends with long life, health and happiness.

Shahid Iqbal

Table of Contents

List of Figures

Abstract

The aim of this research work is to analysis the magnetic properties of silica (SiO_2) coated maghemite (γ-Fe_2O_3) nanoparticles synthesized by using sol-gel. X-ray diffraction (XRD) pattern determined that average crystallite size of nanoparticles was 19 nm, as determined by using Debye Scherrer's formula. FCC inverse spinel structure was also confirmed from the result of XRD analysis. Scanning electron microscopy (SEM) showed that the nanoparticles are spherical in shape. In zero field cooled/field cooled (ZFC/FC) measurements, the average blocking temperature (T_B) of nanoparticles was found to be lower than the room temperature which showed their superparamagnetic nature at room temperature. The saturation magnetization value of SiO_2 coated maghemite nanoparticles was lower than counter bulk maghemite which is attributed to smaller average crystallite size, large surface spin disorder and presence of non-magnetic SiO_2 in nanoparticles. Saturation magnetization (M_s) increases with decreasing temperature due to reduction of thermal fluctuations at low temperatures and M_s also follows the Bloch's law. The coercivity is increased sharply at low temperatures which is due to contribution of large surface anisotropy. Magnetic relaxation showed slow-spin dynamics in both FC and ZFC protocols which ensured the presence of spin-glass behavior in them. The most probable reason of spin-glass behavior is the presence of disorder surface spins. All these measurements showed that amorphous SiO_2 surface coating plays a significant role in changing the structural, morphological and magnetic properties of maghemite nanoparticles.

CHAPTER 1

Introduction

1.1. Nanoscience

The science which deals with the study of manipulation and developments of materials at macromolecular, molecular and atomic level is known as nanoscience [1]. It is the combination of two words nano and science derived from Greeks "Nanos" means "Dwarf", i.e. one billionth part of anything. Word science came from Latin "Scientia" means knowledge [2-3].

1.2. Nanotechnology

A group of technologies which deals with the nano level controlled material structure having noteworthy and useful properties [4-5]. It also deals with preparation, designing and characterization by limiting the material structure, system and devices through holding material size and shape at nanoscale [6]. As we reduce the particle size to nano level surface to volume ratio of the particle increases greatly, quantum confinement effects involved and discreteness of energy bands take place [7]. These effects bring the significant changes in the electrical, optical and magnetic properties of material as equating to larger level. Importance of materials have been increased as their size reduces to range of nanometer and they have very useful and bright properties in case of 0-D, 1-D, 2-D, 3-D. The usefulness of materials are not same as in bulk size [9]. If the body structure of a material limited to nanometer level than we will be able to get the material with new roles and thus increasing the functioning of material. Fig. 1.1 shows the structural image of 0-D, 1-D, 2-D, 3-D nanoparticles.

| Clusters | Nanotubes, fibers and rods | Films and coats | Polycrystals |
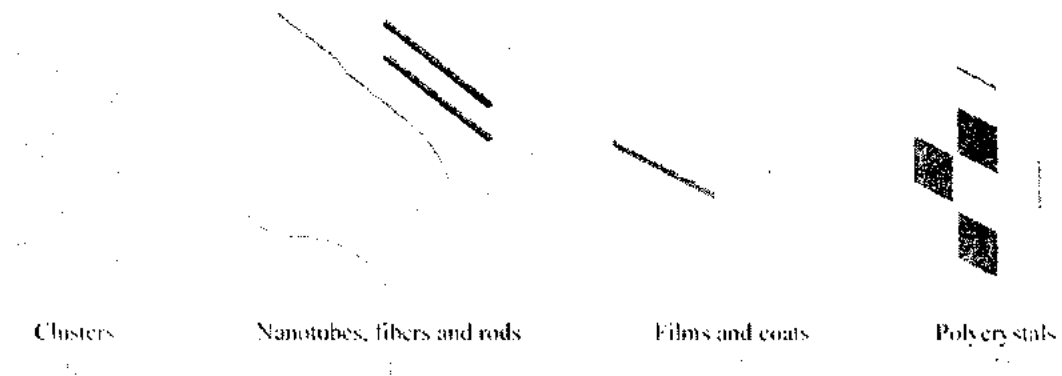
Fig. 1.1: Zero. one. two. and three dimensional nanomaterials [9].

1.2.1. Applications of Nanotechnology

Nanotechnology has wide range of applications in almost all science fields such as Physics, Engineering, Medicine, Chemistry, etc. In nanocrystals variety of properties are increased such as toughness, hardness, ductility, magnetic and electrical properties [10]. Due to the useful working of a nanomaterial they are used in the field of storage device, energy, electronics, solar cell, electrochemistry, environmental, optical, magnetism, fuel cell, nano catalyst, high energy and batteries.

1.2.2. Historical Perspective of Nanotechnology

In ancient times, this technology was used in the field of medicine and pottery. During 2500 BC Chinese and Indian used gold nanoparticles as a drug [11]. In middle Ages, gold was used to make the glasses of churches of different colors and hues and during 16th century in Europe it was thought that colloidal gold in aqueous form can cure many diseases [12]. In 1915, Wolfgang Ostwald wrote a famous book "The World of Neglected Dimensions" in which he accepted the colloidal particles as matter unique state. These particles are so small that they can no longer be recognized microscopically, while they are still too large to be called molecules. The term "nanotechnology" was used first time by Norio Taniguchi (1912-1999) in 1974 in a technology of production paper [13-14]. The growth of nanotechnology started when Professor Richard Feynman at the yearly meeting of American Physical Society at Caltech in 1959, highlighted the worth of it by saying that "There is a plenty of room at the bottom" [15-16] and due to this foresight and visionary thinking Feynman is often referred as father of nanotechnology [17]. Later on Eric Drexler wrote a book "Engines of Creation: The Coming Era of Nanotechnology" in which he explain in detail nanotechnology potentials, its concepts and even dangers too. This book brought Feynman's vision to a broader audience [18].

1.3. Nanoparticles

According to British Standards nanoparticles are defined as "Nanoparticles are the particles with one or more dimensions at the nanoscale" and suggested the nanoscale is in the range of 1-100 nm or less [19]. A nanoparticle is an object that acts in term of functioning and transport as a whole unit. It has different forms like, colloids, nanocrystals and clusters. As compared to bulk the nanoparticle have very assuring properties such as optical, mechanical, electrical and magnetic as the size going to decreases under 20 nm. Ferromagnetism of a particle changes towards superparamagnetism because of high surface to volume ratio which raised the surface energy [20-21].

2

Mainly two approaches (top-down and bottom-up approaches) are used for the synthesis of nanoparticles. In top-down approach breaking of bulk material into nano size material takes place that involves different techniques like high energy milling and sputtering techniques, etc. The bottom-up approach deals with atom by atom, cluster by cluster to manufacture bulk size material that involves sol–gel method, solution combustion method, etc. as shown in Fig. 1.2.
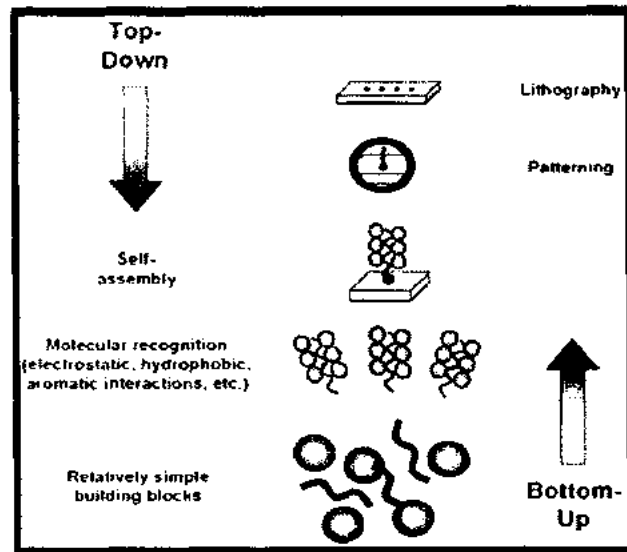
Fig. 1.2: Schematic variety of nanostructure synthesis and assembly approaches [22].

1.4. Concepts of Magnetism

Magnetism concerns to the physical process which arises due to force among the magnets. These objects develop a field that pull or repel other objects [23]. Firstly, 2500 years ago this phenomenon was observed in the iron mineral magnetized pieces in the old city of magnesia (Mantissa in western Turkey is its new name).

Magnetization is a process that makes a substance permanently or temporarily magnetic and is symbolized by "M" [24].

The magnetic flux density is written as,

$$B = \mu H \qquad (1.1)$$

In which "H" is applied magnetic field. "μ" is permeability of the solid material and "B" is magnetic flux density.

$$\mu = \mu_0 \mu_r \qquad (1.2)$$

In eq. (1.2) "μ_r" is the Relative permeability of the medium and "μ_0" is the Permeability for free space having value $4\pi \times 10^{-7}$ H-m^{-1}.

After putting the value of Eq. (1.2) in Eq. (1.1), we acquire

$$B = \mu_o\mu_r \, H \qquad (1.3)$$

By adding $\mu_0 H$ on both sides of eq. (1.3) and after simplification, we acquire,

$$B + \mu_o H = \mu_o\mu_r H + \mu_o H$$

$$B = \mu_o H + \mu_o\mu_r H - \mu_o H$$

$$B = \mu_o H + \mu_o H \, (\mu_r - 1)$$

$$B = \mu_o H + \mu_o M \qquad (1.4)$$

In above eq. (1.4), magnetization (M) is equal to H (μ_r-1).

As we know

$$\chi_m = \mu_r - 1$$

Here "χ_m" is magnetic susceptibility and it is dimensionless quantity. So magnetization can be written as

$$M = \chi_m H \qquad (1.5)$$

Eq. (1.5) expresses clearly that magnetization is proportional to the magnetic field intensity. When current flows in a loop then magnetic field "H" is produced at its center as shown in Fig. 1.3.
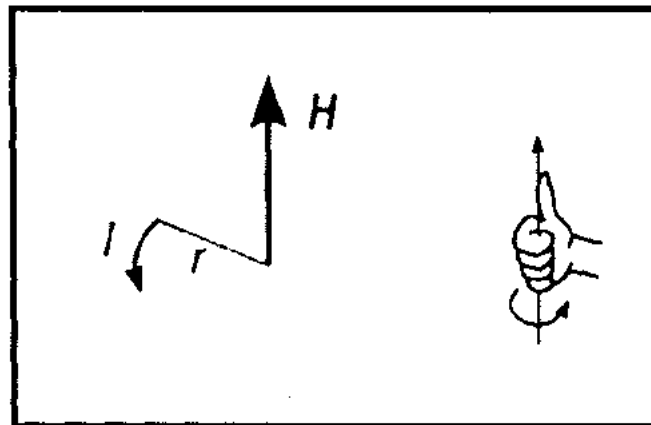
Fig. 1.3: Magnetic field generated by current loop [26].

4

Magnetic field is evaluated in Oersted (Oe) or A-m^{-1} [25]. When we employ magnetic field in vacuum then magnetic flux density is related to field intensity as B=μ_0H. In the case of magnetic solid "B" and "H" are related as,

$$B = \mu_o(H + M)$$ (1.6)

As we know "M" is proportional to "H" for a linear medium.

So,

$$M = \chi_m H$$ (1.7)

By putting the value of eq. (1.7) into eq. (1.6) than we acquire the eq. as given below,

$$B = \mu_o (1 + \chi_m) H$$ (1.8)

As we know μ_r=1+χ_m so eq. (1.8) become as.

$$B = \mu_o \mu_r$$ (1.9)

The above eq. (1.9) clearly shows the linear relationship b/w applied magnetic field and magnetic induction.

1.4.1. Magnetic Dipoles

Naturally existing magnetic materials are dipolar. According to Maxwell relation, i.e. divB = 0, in nature no monopole exists. Magnetic and electric dipoles are similar to each other [27]. As shown in Fig. 1.4.
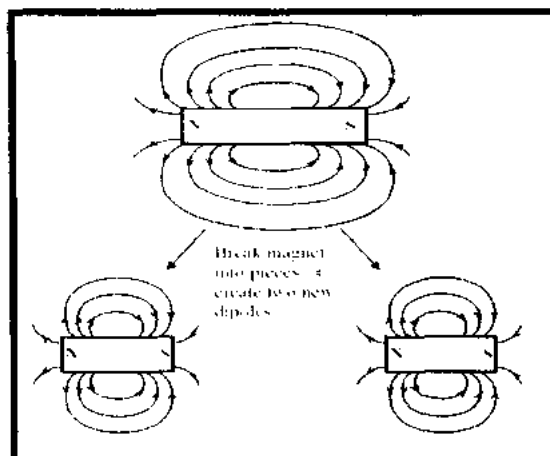
Fig. 1.4: Poles of a magnet [28].

5

1.4.2. Sources of Magnetic Moment

Magnetic dipole moment is essential for magnetism in a material and are originates due to electron's spin and orbital motion in an atom as shown in Fig. 1.5.
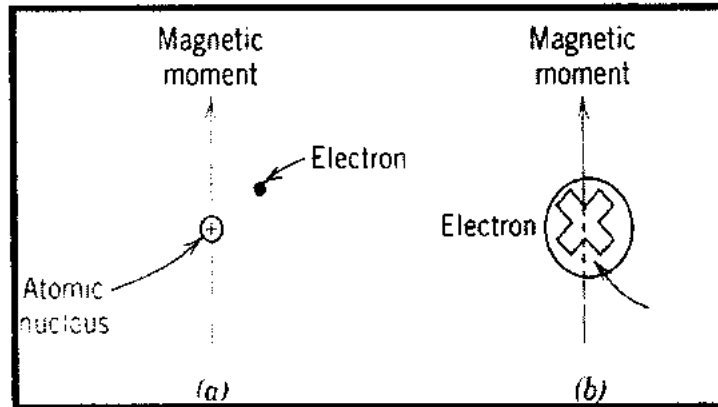
Fig. 1.5: (a) Orbital magnetic moment and (b) spin magnetic moment [29].

Because of these orbital and spin magnetic moments electron is thought as little magnet. The size of magnetic moment is showed by a unit known as Bohr magnetron and represented by the symbol "μ_B". The value of a Bohr magnetron (μ_B) is 9.27×10^{-24} A-m^2. According to this term spin magnetic moment of all electrons influenced by an atom is $\pm \mu_B$. Here "+" shows spin up and "-" shows spin down. In term of Bohr magnetron orbital magnetic moment is "$m_l\mu_B$". Here "m_l" is the magnetic quantum number.

1.5. Magnetic Materials

Those materials which give response when they are placed in an external magnetic field are known as magnetic materials. Due to the orientation of the magnetic dipole moment materials are classified into five major types as written below,

- Diamagnetism.
- Para magnetism.
- Ferromagnetism.
- Antiferromagnetism.
- Ferrimagnetism.

1.5.1. Diamagnetism

Materials having paired electrons are known as diamagnetic materials and net magnetization of these materials is zero e.g. neon, nitrogen, hydrogen, helium, lead, copper,

etc. [30]. Fig. 1.6 shows the diamagnetic material response (a) without fields and (b) with applying fields.

Diamagnetic Materials
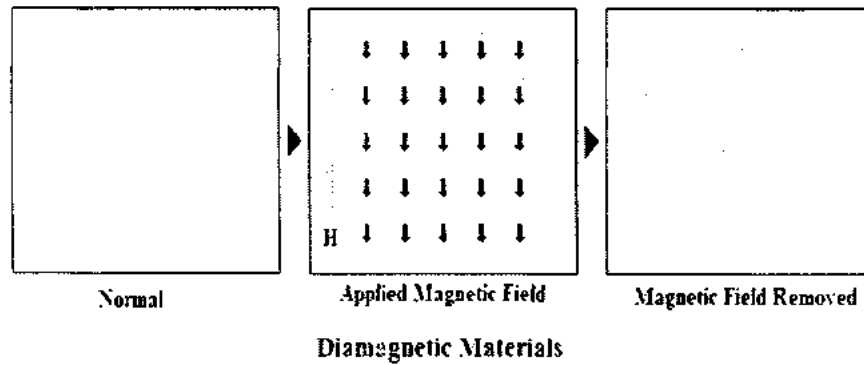
Fig. 1.6: Diamagnetic materials (a) when no field is applied (b) when field is applied [31].

Diamagnetic materials have negative susceptibility due to opposing of induced magnetic moment to external field and it is independent of temperature as shown in Fig. 1.7.
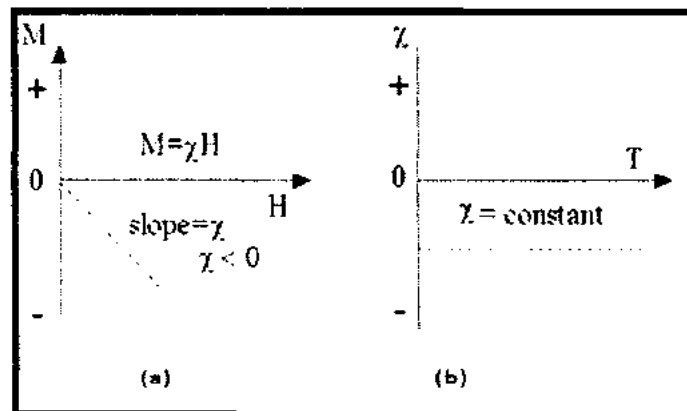
Fig. 1.7: (a) Behavior of magnetic susceptibility of diamagnetism with applied magnetic field (b) with temperature [32].

1.5.2. Paramagnetism

In these materials partially filled orbital's show paramagnetic properties and due to unpaired electrons magnetization develops in these materials. They show magnetization when external field is applied because magnetic moments are adjusted in an applied field direction and finally net magnetic moment is in the field direction [33] But they show zero magnetization when field is removed due to magnetic moment's random alignment. Fig. 1.8 represents magnetic response of paramagnetic materials with and without external applied field.

7
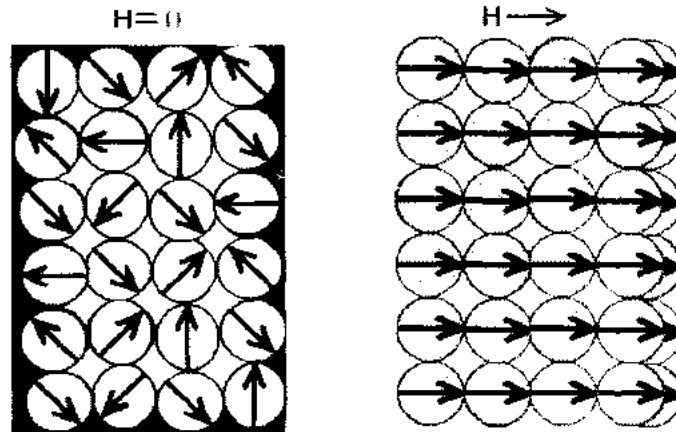
Fig. 1.8: Paramagnetic materials with (a) no magnetic field (b) with applied magnetic field [34]

Liquid oxygen, chromium, strontium, platinum are the examples of paramagnetic materials.

Curie law fits on paramagnetic material. According to law magnetization and temperature are inversely proportional to each other [35-36].

Mathematically it can be written as,

$$M = C.B/T \qquad\qquad (1.10)$$

In above equation C is constant.

In paramagnetic material external applied field works independently on each atomic dipole that's why they do not give long-range order and show small positive magnetic susceptibility ($\chi\approx0$) [37].

1.5.3. Ferromagnetism

Ferromagnetism is a characteristic of a material which originates in the absence of external applied magnetic field due to spontaneous magnetization [38]. When external field is removed alignment remains due to the exchange interaction [39]. When the material is large there is set of domains in it which are separated by a wall known as domain wall of thickness nearly 100 atoms [40]. In ferromagnetic material each domain has unpaired electrons whose spins are parallel to each other. In the absence of external field net magnetization of material is zero due to the random alignment of domains. When the external field is applied domain's magnetic dipoles aligned themselves in the field direction and give maximum magnetization. Examples of ferromagnetic material are iron, nickel, cobalt, etc. Fig. 1.9 shows the magnetic response of a ferromagnetic material with and without applied external field.

(a) Unmagnetized domains   (b) Magnetized domains
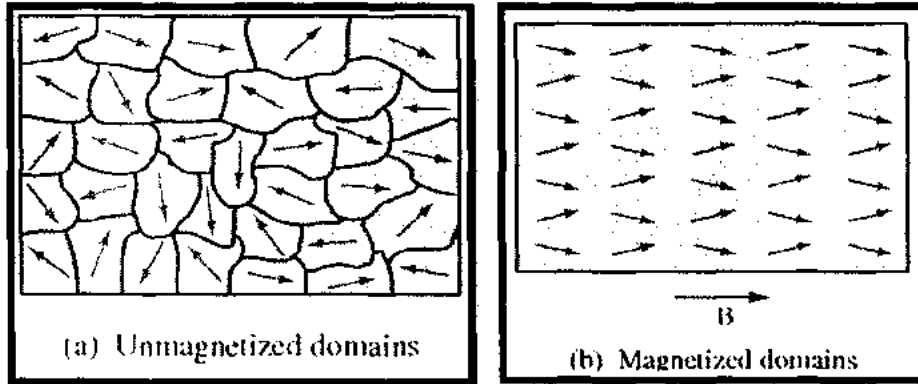
Fig. 1.9: Ferromagnetic (a) magnetic domains without field and (b) domains with applied magnetic field [41].

1.5.3.1. Curie Temperature

In 1895, Pierre Curie state the Law that relates magnetic properties to change in temperature which is called Curie point and temperature at that point is known as Curie temperature. At that temperature the saturation magnetization of ferromagnetic material disappears due to thermal energy and the material shows paramagnetic behavior [42].

Mathematically it can be written as:

$$\chi = C/(T - T_c) \qquad (1.11)$$

In above eq. (1.11) T_c = Curie temperature, T = temperature, C = Curie constant and χ shows magnetic susceptibility. Below Curie temperature, a strong interaction exist b/w the parallel alignment of magnetic moments of domains but when we apply thermal energy at Curie temperature which minimizes the coupling energy that's why ferromagnetic material behaves as paramagnetic material [43] as shown in Fig. 1.10.
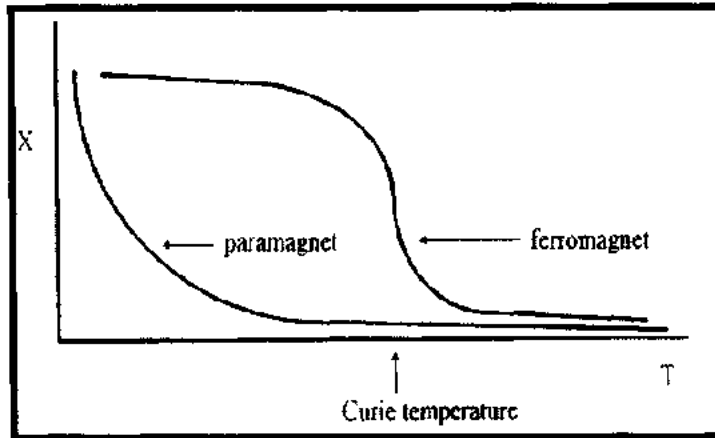
Fig. 1.10: Effect of temperature upon magnetic materials [44].

1.5.3.2. Hysteresis

Hysteresis is the property of ferromagnetic materials that maintains the applied magnetic field memory and this phenomenon is shown in Fig. 1.11.
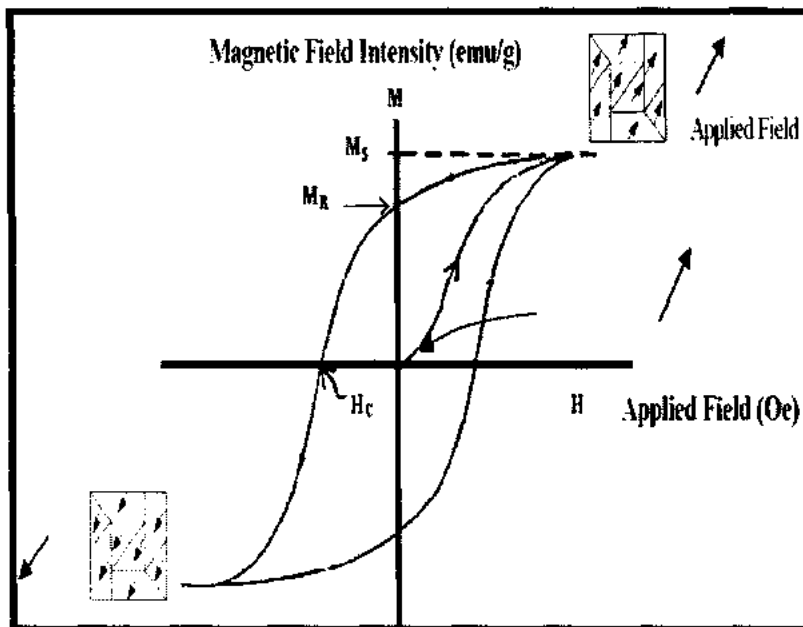
Fig. 1.11: Hysteresis loop [45].

Terms which are related to hysteresis are described below,

10

1.5.3.3. Saturation Magnetization

It is the point at which maximum magnetization is achieved by the applying a large magnetic field as a result maximum spins alignment takes place and beyond this point no more alignment of spins can occur [46]. It is symbolized by "M_s" as shown in Fig. 1.11.

1.5.3.4. Remanent Magnetization

When the applied magnetic field is removed then the magnetic spins alignment stops and value of net magnetization decreases. At zero field. i.e. H = 0 material show some degree of magnetization. This magnetization is known as remanent magnetization which is symbolized by "M_r" [46] as shown in Fig. 1.11.

1.5.3.5. Coercivity

Coercivity is the intensity of magnetic field to reverse magnetization of permanent magnets. Materials having high coercive force need high magnetic field to magnetize or demagnetize. The value of applied magnetic field which is required to reduce magnetization to zero is called Coercivity which is symbolized by "H_c" [46] as shown in Fig. 1.11. Coercivity varies with material grain structure and composition. and could be tune by cold working and annealing.

1.5.4. Antiferromagnetism

Antiferromagnetism is the characteristic of a material which originates due to the anti-parallel alignment of magnetic moments b/w neighboring atoms in the absence of external magnetic field. Due to the opposite spinning of electron anti-ferromagnetic materials does not give magnetization. Crystal which gives this type of response has two types of sub lattices and which are the main cause for this type of response. Both lattices give the spontaneous magnetization in opposite direction to one another [47] as shown in Fig. 1.12.

11
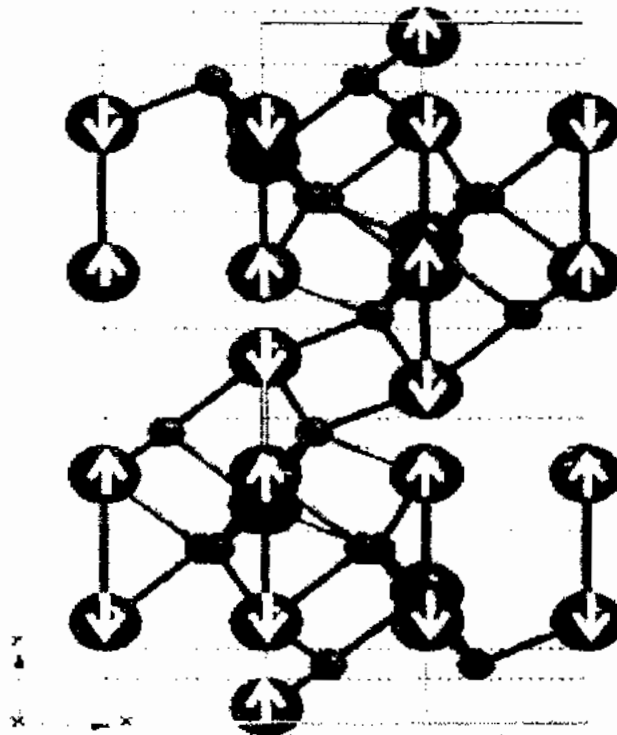
Fig. 1.12: Antiferromagnetism due to opposite sub lattices spins [48].

1.5.4.1. Neel Temperature

Neel temperature is the temperature for antiferromagnetic material below which there is a spontaneous anti parallel coupling of atomic magnets. It is also known as magnetic ordering temperature and symbolized by "T_N". But above this temperature magnetic ordering goes on reducing.

Mathematically their relation can be expressed as:

$$\chi = C/(T - \theta) \tag{1.12}$$

In above eq. (1.12), T= temperature. θ =T_N = Neel temperature, χ = magnetic susceptibility and "C" is Curie constant. Above the T_N, antiferromagnetic material behave as paramagnetic material because the thermal energy is enough to randomly fluctuate the oppositely aligned atomic moments and leads to vanishes the long-range order [49] as shown in Fig. 1.13.

12
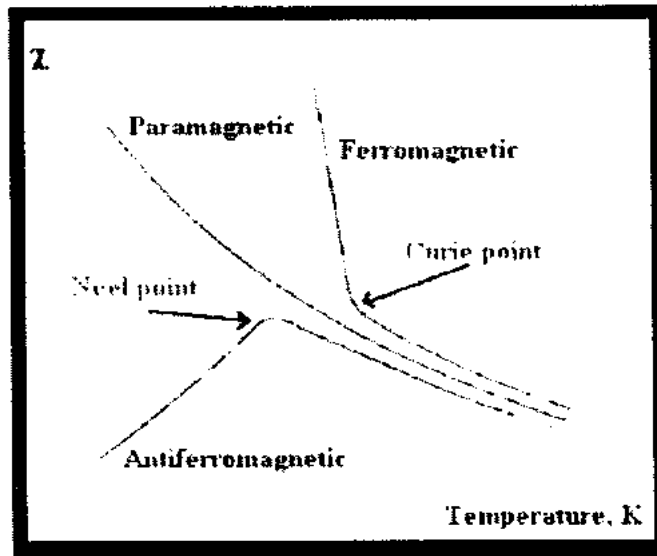
Fig. 1.13: Effect of temperature upon magnetic materials [50].

1.5.5. Ferrimagnetism

Ferrimagnetism is the characteristic of the material in the absence of external applied field in which the magnetic moments of two sub lattices arranged anti-parallel to each other and the magnitude of magnetic moments are not equal. Due to the partial cancellation, material shows a net magnetization as expressed in Fig. 1.14.
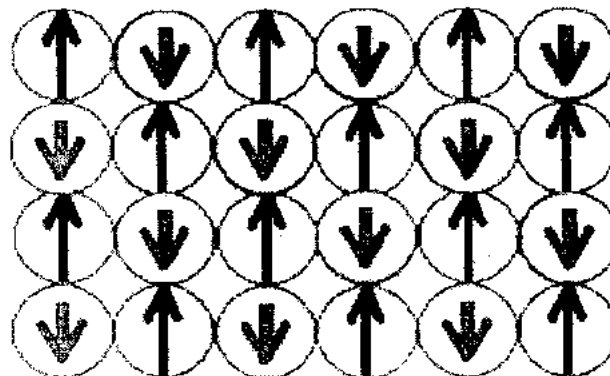
Fig. 1.14: Ferrimagnetic behavior with unequal and opposite magnetic moments [51].

Ferrimagnetic material produced all types of hysteresis loop related terms as ferromagnetic material but the difference b/w them is they have different magnetic ordering.

1.6. Magnetic Anisotropy

The dependence of material magnetic properties on a preferred direction is called magnetic anisotropy. The energy related with the spins alignment mathematically written as,

13

$$E_A = KV sin^2 \theta \hspace{3cm} (1.13)$$

In eq. (1.13), K= magnetic anisotropy, V= volume of particle, E_A = energy barrier and θ is the angle between the easy axis and magnetic moment. In which easy axis is the direction along which small applied field is enough to attain the dipoles total magnetization of given material [52]. Magnetic anisotropy controls the remanence. coercivity and strongly affects the hysteresis loops shape [53].

1.6.1. Magneto Crystalline Anisotropy

Magneto crystalline anisotropy depends on crystal structure and independent of shape and grain size. it is the energy needs to deflect the magnetic moment from easy to hard direction in a single crystal. These directions, i.e. easy and hard originate from spin-orbit coupling [54].

1.6.2. Stress Anisotropy

In addition to magneto crystalline anisotropy, another effect known as magnetostriction is due to the spin-orbit coupling. In 1842, Joule observed magnetostriction. When a sample is magnetized in a preferred direction he observed strain in this preferred direction. This strain is related to the stress on that specimen. Anisotropy energy depends upon that stress state of specimen.

1.6.3. Surface Anisotropy

The surface atoms have lower symmetry comparing to the atoms in particle and effect of surface atoms on energy of particle depends upon magnetization orientation. This develops the surface anisotropy. As the particle size reduces its contribution to magnetic anisotropy increases.

1.7. Single Domain Particles

Single domain particles are defined as "A particle in which the every spin is of at the same direction therefore the total magnetic moment is the sum of all the spins". In ferromagnetic material the size of domains is larger so the particle with uniform magnetization at any field is single domain particle.

Their magnetic moment can be written as,

$$ms = MsV \hspace{3cm} (1.14)$$

Here M_s = saturation magnetization. V = particle volume.

14

Coercivity depends upon the size of domain as shown in Fig. 1.15.
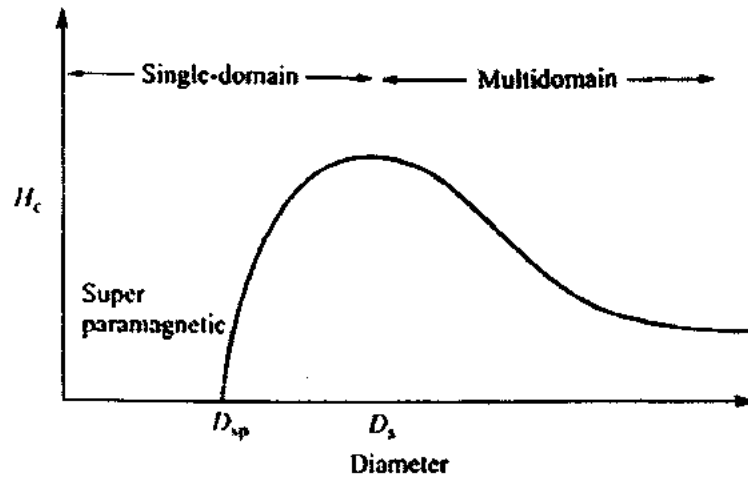
Fig. 1.15: Coercivity as a function of particle sized (D_{sp} is the superparamagnetic size and D_s is the single domain particle size) [55].

1.8. Superparamagnetism

The magnetic anisotropy is generally proportional to the volume of the particle which holds particle magnetized in a preferred direction [56]. As particle size reduces under the 10 nm then energy related to the uniaxial anisotropy (K) decreases as much that thermal energy is enough to overcome any preferred orientation of particle moment. A single domain particle that attains magnetization equilibrium in short time proportional to the measurement time at experimental temperature is referred to as super paramagnetic as shown in Fig. 1.16.
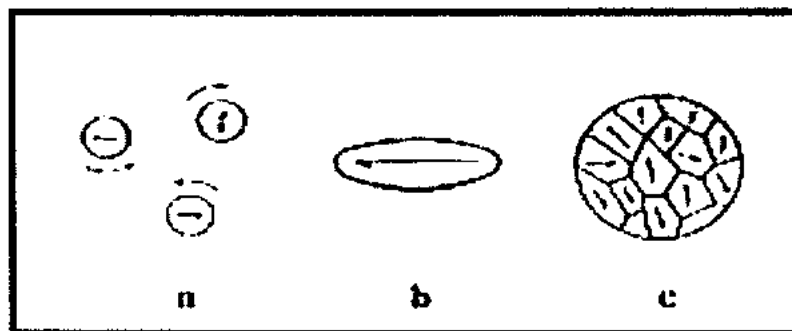
Fig. 1.16: Domain structures observed in magnetic particles: a) superparamagnetic; b) single domain particle; c) multi-domain particle [57].

15

1.8.1. Magnetic Relaxations Observed in Superparamagnetic Particles

When external field is applied then particles magnetic moments are align in field direction through particle rotation and moment. When external magnetic field is removed the frequency of thermally activated is given by the equation as,

$$f = f_0 e^{-E/kT} \qquad (1.15)$$

Here $f_0 =$ attempt frequency which is $10^9 \, s^{-1}$. Here frequency is the rate at which particles gets thermal equilibrium [58]. Energy barrier for the relaxation time of nearly 100 s to attain thermal equilibrations is,

$$\Delta E_{crit} = in(t/o) \, KT = 25 KT \qquad (1.16)$$

Where $\Delta E = KV$. The conditions for superparamagnetism are observed and for a particle mathematically defined as,

$$KV = 25 \, k \, T \qquad (1.17)$$

In which kT = thermal energy, V = volume of particle and K is the anisotropy energy constant [59]. Particles with size larger than critical size and relaxation time more than 100 s are named as blocked [60].

1.8.2. Blocking Temperature

The blocking temperature (T_B) of a material is the temperature above which particle show superparamagnetic behavior because $KV < 25 \, kT_B$ and below this temperature particle anisotropy blocks the freely movement of moment and condition at blocked state is $KV > 25 \, kT_B$ [61]. Mathematically it can be written as,

$$T_B = \frac{KV}{25 \, k} \qquad (1.18)$$

1.9. Ferrites

These are chemical compounds which are formed by the reaction of iron oxide into a magnetic material. Ferrites are brittle and hard. They belong to the family of ferrimagnetism. The general chemical formula for ferrites is KFe_2O_4. Where K is represents the divalent elements [62]. This includes Mn, Co. Fe. Zn and Ni. Iron is too considered in ferrites. Ferrites are classified into two types on the behalf of their magnetic properties as given below,

- Soft ferrites.

16

- Hard ferrites.

1.9.1. Soft Ferrites

Soft ferrites are normally ferromagnetic materials and having cubic crystal structure. These materials have small hysteresis loops and low coercivity. The direction of magnetization of soft materials can easily be changed by applying small amount of field. The chemical formula for soft ferrites is $MOFe_2O_3$, in which M denotes transition metal such as zinc, nickel and iron. In soft materials domain wall motion takes place easily through proper annealing due to small number of impurities and dislocations [63].

1.9.2. Hard Ferrites

Naturally hard ferrites are permanent magnets. These are oxides of strontium, iron and barium. Hard ferrites have larger coercivity values and high remanence when field is applied. When these materials are magnetically saturated they have high magnetic permeability. Therefore hard ferrites have high power to store magnetic fields for several applications such as loud speaker, telephone, generators and motors.

1.10. Spinel Ferrites

Spinel ferrites have cubic crystal structure with general formulation $A^{2+}B_2^{3+}O_4^{2-}$ in which the oxide anions arranged in a cubic close packed lattice and the tetrahedral and octahedral sites in lattice are occupied by cations A and B. In general formula A and B represent the divalent, trivalent metal ions, including magnesium, zinc, iron, manganese, aluminum, chromium, titanium and silicon. There are 32 octahedral and 64 tetrahedral lattice sites are present in unit cell of spinel ferrite. The crystal structure of spinel ferrite in shown in Fig. 1.17.

Oxygen
- B-atoms octahedral site
- A- atoms tetrahedral site
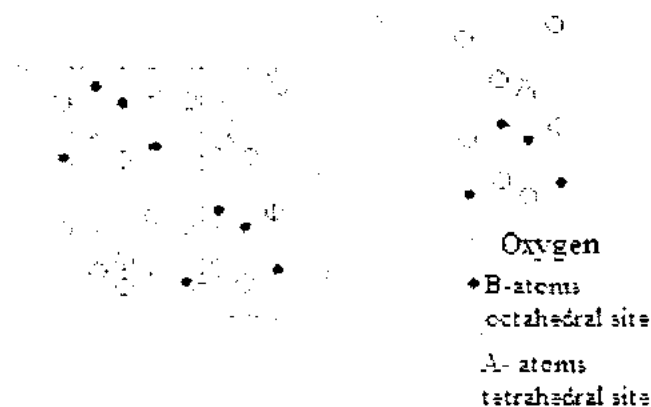
Fig. 1.17: Crystal structure of AB_2O_4 spinel ferrite [64].

17

1.10.1. Types of Spinel Ferrites

Spinel ferrites are classified into three different types on the basis of their octahedral and tetrahedral lattice sites positions as given below

- Normal spinel ferrites.
- Inverse spinel ferrites.
- Mixed spinel ferrites.

This thesis is focus on the normal spinel ferrites because main purpose of my research work is the study of the magnetic properties of iron oxide phase that is maghemite. It is an example of normal spinel ferrite.

1.10.1.1. Normal Spinel Ferrites

Normal spinel structures are consist of two different types of lattices known as tetrahedral the site A and octahedral site B. Formula of normal spinel ferrite is $(M)^{tet} [Fe_2]^{oct} O_4$, where metallic ions lying at tetrahedral site (A) are represent by M and Fe represent the iron ions lying at octahedral site (B). In normal spinel ferrites, there are 16 octahedral and 8 tetrahedral sites are occupied by metallic ions.

1.10.1.2. Inverse Spinel Ferrites

In inverse spinel structure the tetrahedral site are completely filled by Fe^{3+} ions, whereas at octahedral site both M^{2+} and Fe^{3+} ions are randomly present. Chemical formula of inverse spinel ferrite is $(Fe_2)^{tet} [Fe_2.M]^{oct} O_4$. Spinel ferrites are ferrimagnetic in nature. An example of spinel ferrite is Fe_3O_4 in which divalent cation Fe is present at octahedral (B) site. The inverse spinel structure of maghemite is shown in Fig. 1.18.
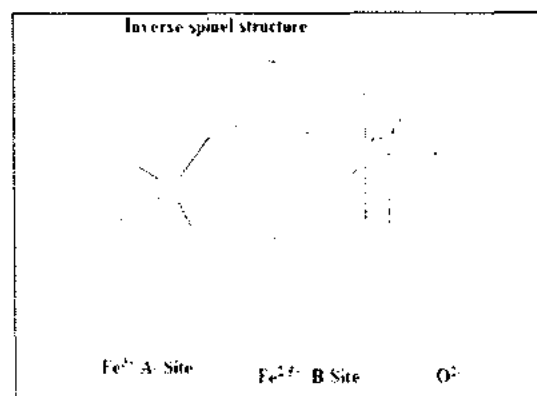
Fig. 1.18: Inverse spinel structure of maghemite [65].

The main purpose of this thesis is the study of the magnetic properties of maghemite (Iron Oxide phase). It is inverse spinel ferrite.

1.11. Iron Oxide Nanoparticles

Nanoparticles of iron oxide with diameter range between 1-100 nm are known as iron oxide nanoparticles [66]. They are regarded as ferrite and have noteworthy applications in wide variety of fields. Iron oxide nanoparticles gain interest not only because of its fundamental properties but also due to their super paramagnetic, low Curie temperature, high force, high magnetic susceptibility etc. [67-68]. Due to presence of Fe (II/III) ions in iron oxide nanoparticles they have biological compatibility and non-toxicity [69-70]. Iron atoms has strong magnetic moment because of having 4 unpaired electrons in 3d shell, while Fe^{3+} has 5 unpaired electrons and Fe^{2+} has 4 unpaired electrons in 3d shell. Hence when crystals are made up from these Fe^{3+} and Fe^{2+} ions or iron atoms they can be in ferrimagnetic, antiferromagnetic or ferromagnetic state [70]. Iron oxides exist in variety of structures. It shares its crystal structure with various minerals such as Ni, Co or Cu. In the structure of iron oxide nanoparticles hydroxides ions or oxygen plays a prominent role. Iron oxide is chemical compound which is constructed by oxygen and iron and occur in a wide variety of settings which are given below.

Hydroxides Phase

- Iron (Fe^{+2}) hydroxides {$Fe(OH)_2$}
- Iron (Fe^{+3}), Bernalite {$Fe(OH)_3$}

Oxides Phase

- Epsilon phase (ε-Fe_2O_3)
- Gamma phase (γ-Fe_2O_3), Maghemite
- Beta phase (β-Fe_2O_3)
- Alpha phase (α-Fe_2O_3), Hematite
- Iron (Fe^{+3}) oxides (Fe_2O_3)
- Iron (Fe^{+2}, Fe^{+3}) oxides, (Fe_3O_4), Magnetite
- Iron (Fe^{+2}) oxide, (FeO), Wustite

Oxides/ Hydroxides Phase

- Ferrihydrite phase ($5Fe_2O_3.9H_2O$)
- Feroxyhyte phase (δ- FeOOH)

- Lepidocrocite phase (γ-FeOOH)
- Akaganeite phase (β-FeOOH)
- Goethite phase (α-FeOOH)

1.12. Maghemite Nanoparticles

Maghemite has extra ordinary optical, electrical, and magnetic properties and its main advantage is its chemical stability [71-72]. Maghemite is superparamagnetic at room temperature when the particle size is less than 10 nm [73].

1.12.1. Crystal Structure and Properties

Maghemite is a typical inverse spinal ferrite has same crystal structure as magnetite with Fe (II) - deficiency. The formula unit of maghemite is $(Fe^{+3})_A[Fe_{40/3}^{+3} \Delta_{8/3}]_B O_{32}$, where Δ symbolizes vacancy and A and B represent tetrahedral and octahedral lattice sites [74]. Maghemite has a cubic crystal structure and its value of "a" is 0.833 nm. Fe^{3+} cations which are arbitrarily distributed in 16 octahedral and 8 tetrahedral interstitial sites in the FCC packing of oxygen anions and vacancies Δ are located in the octahedral sites [75]. Maghemite crystal structure is shown in Fig. 1.19.
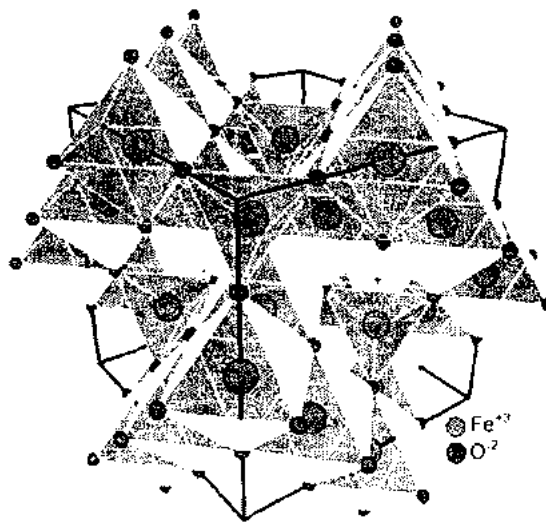
Fig. 1.19: Maghemite crystal structure [76].

Maghemite displays ferrimagnetism and has reddish brown colour. Its density (g/cm^3) is 4.87. The magnetic susceptibility (emu/g) is 76 - 81 and Curie temperature (K) is 820 – 986 [77-78]. Magnetic properties are generally divided into intrinsic and extrinsic properties. Interinsic properties such as magnetocrystalline anisotropy (K) and saturation magnetization (M_s)

depends on materials and extrinsic properties such as remanence (M_r) and coercivity (H_c) rely on the method the material is fabricated [79].

1.12.2. Uses of Maghemite Nanoparticles

Maghemite has a very wide range of useful and interesting applications. In the medical field it is used in cell separation, DNA analysis, active and passive targeting, and in preparation of biocompatible magnetic fluids [80]. In magnetic resonance imaging (MRI) maghemite is used as magnetic contrast agent and also used in diagnosis and drug delivery [81]. In the technological field it is used as optical power limiting agent, magnetic recording media, magnetic refrigeration, and magnetic sensors. It is used in preparation of ferro-fluids [82].

1.13. Role of Silica Coating/Matrix

In the synthesis of nanoparticles the agglomeration is a big obstacle. In order to reduce particles agglomeration magnetic materials are coated with non-magnetic material such as Al_2O_3 or SiO_2. We prefer SiO_2 as controlling agent over other non-magnetic material because it is highly biocompatible, thermally stable and non-toxic in nature [83]. In order to improve the magnetic properties silica has given preference because it improves stability of dispersions of nanoparticles during synthesizing process and also modifies the surface. Silica is used to control inter-particle interaction within the solution through shell thickness [84-85]. In this process silica restricts the growth of maghemite nanoparticle to reduce agglomeration. The surface coating of magnetic nanoparticles can influence size, magnetization reversal, blocking temperature, and magnetic relaxation of the nanoparticles.

CHAPTER 2

Literature Review and Synthesis Techniques

2.1. Literature Review

Milivojevic *et al.* [86] examined the magnetic and structural properties of ultra-small magnetic nanoparticles consists of organic ester shell and inorganic iron oxide core dispersed in organic fluid by using polyol route for synthesizing. With the help of XRD they studied that nanoparticles are crystalline and clearly separated. They also studied that at low temperature the particle shows their superparamagnetic behavior and magnetic properties are dependent on the nanoparticles size. The peaks of AC susceptibility and ZFC/FC are at blocking temperature T_B < 12 K. They noted that nanoparticles surface has an important effect on their behaviors.

Nadeem *et al.* [87] investigated the effects of coating and its concentration percentage on the magnetic, dielectric, structural properties and size of maghemite nanoparticles. They used sol–gel method for the synthesis of bare and different weightage silica coated maghemite nanoparticles. They examined the cubic inverse spinel structure of the samples with x = 0, 15 and 30%, and those with higher concentration give amorphous behavior through XRD analysis. They confirmed the formation of phases of maghemite and SiO_2 by Fourier transform spectroscopy. They studied that as SiO_2 concentration increases average crystallite size go on decreasing and due to increase in coercivity saturation magnetization drastically decreases.

Seraj *et al.* [88] utilized the ex situ (post-synthesis) method for the fabrication of gamma-Fe_2O_3/polyrhodanine core/shell nanoparticles with crystallite size of 8 and 1.5 nm is the layer thickness. They used XRD, TEM, FTIR spectroscopy and VSM for the investigation of size, morphology, chemical structure and magnetic properties. Moreover through VSM analysis they noticed that fabricated core/shell nanoparticles give superparamagnetic behavior. They also studied that with the variation in amount of polyrhodanine magnetization of nanoparticles decreases very slightly.

Carvalho *et al.* [89] investigated that magnetic properties and composition of nanoparticles are assumed to depend on their size. They used two different method reduction-precipitation method in open environment and precipitation method in particular environment as a result they attained mean diameter of 7 to 20 nm. For the analysis of sample they used SQUID-magnetometry, XRD and TEM for magnetic, structural and morphological properties,

22

respectively. They studied that iron oxide nanoparticle's composition and their magnetic behavior directly linked with their size.

Deraz et al. [90] synthesized the iron oxide nanoparticles by using combustion method with different fuel ratio and investigated that morphological, crystallite size, crystalline phases and magnetic properties can be handled by the amounts ratio of fuel and metal nitrate while preparing. By XRD analysis they studied the transformation of phases in Fe_2O_3 nanoparticles at different glycine concentration. Through vibrating sample magnetometer analysis the magnetic properties shows that the increasing trend of M_r/M_s ratio, H_c, M_s and M_r totally depends on phase transformation and/or crystallinity improvement of the studied oxides.

Nadeem et al. [91] studied the preparation of single-phase spinel $NiFe_2O_4$ and magnetic properties and influence of several chemical phases on magnetic activity. They used sol–gel method for the synthesis of $NiFe_2O_4/SiO_2$ nanoparticles and as a result gets the particle size in the range of 16–27 nm. Generally the sol–gel method prepares the multi-phase nanoparticles but here they used sol-gel method for single phase nanoparticles. After annealing the sample from 300-900 °C and by using different analysis techniques (XRD, FTIR, and SQUID magnetometry) they studied that how various chemical phases are transformed to single phase spinal structure. They investigated that under 900°C the chemical phases formed was NiFe. NiO. γ-Fe_2O_3, α-Fe_2O_3, and $NiFe_2O_4$, respectively. They also studied that the opposite trend of (coercivity vs. annealing temperature) and (saturation magnetic moment vs annealing temperature) clearly distinguishes the different phases of metallic, antiferromagnetic, and single-phase spinel $NiFe_2O_4$.

Tuutijärvi et al. [92] investigated that γ-Fe_2O_3 nanoparticles are special adsorbent because of good adsorption capacity and magnetic properties which is used for the removal of As(V) from water. They Synthesized maghemite nanoparticles with sol-gel process and mechanochemical method. They prepared commercially available maghemite nanoparticles with size variation from 3.8 to 18.4 nm and noted that all these particles are productive to remove As(V) from water. They assumed that adsorption capacity depends upon the pH effect and nanoparticles particular surface area. They characterized the maghemite nanoparticles by XPS, XRD, VSM. TEM, Zeta and BET potential analyzers and the characterization showed that all γ-Fe_2O_3 nanoparticles had crystalline phase having cubic structure.

Drbohlavova et al. [93] looked into the preparation and magnetic properties of iron oxides and gadolinium nanoparticles. They used water in oil micro emulsion and co-precipitation method for the synthesis of gadolinium and iron oxide nanoparticles. Through XRD they studied Fe based nanoparticles give crystalline phase and Gd based nanoparticles. They studied the different hysteresis loops and coercivities of the sample. They noticed that difference of saturation magnetization is due to the chemical and phase composition of nanoparticles.

Zhao et al. [94] investigated the production and magnetic properties of cobalt ferrite ($CoFe_2O_4$) (80 wt. %) nanoparticles which dispersed in SiO_2 matrix. They synthesize the $CoFe_2O_4$ nanoparticles by sol-gel method and annealed at 800–1000 °C temperature. When the particle size was 30 nm they examined maximum coercivity value for both uncoated and silica-coated $CoFe_2O_4$ nanoparticles and this was due to single domain coherent rotation. They investigated that silica restricts the development of $CoFe_2O_4$ nanoparticles and the coercivity of silica coated cobalt ferrite nanoparticles increased while saturation magnetization were reduced. They also studied that due to multi domain behavior the coercivity of larger size nanoparticles while for smaller size nanoparticles reduction in coercivity was due to the superparamagnetism.

Zhang et al. [95] investigated the preparation and magnetic properties of silica coated cobalt ferrite nano composites. They used sol-gel method for the synthesis of $CoFe_2O_4/ SiO_2$. Through analysis of sample they studied that dry gel must be annealed at more than 400 °C to attain single phase $CoFe_2O_4/ SiO_2$ nanoparticles. They noticed that size of cobalt ferrite nanoparticles can be controlled by annealing temperature and by increasing the cobalt ferrite concentration in silica the value of saturation magnetization increases accordingly.

Fiorani et al. [96] investigated that the surface effects and inter-particle interactions plays a prominent role in the dynamic and static properties of γ-Fe_2O_3 nanoparticles with average diameter (D) = 2.7, 4.6 and 8.7 nm in powder form. They studied the AC susceptibility and magnetization at variable frequency (5<v<104 Hz) and utilized Mossbauer spectroscopy to measure the dynamic and static magnetic properties of powders. They studied that surface effects have an important role in determining the final magnetic state of nanoparticle.

2.2. Synthesis of Ferrite Nanoparticles

There are various experimental techniques for the preparation of nanoparticles to control their shape and size. Each experimental technique has its own advantages and disadvantages and limitations depending on synthesis conditions. For the synthesis of iron- ferrite

24

nanoparticles there are two main experimental techniques and lots of sub experimental techniques which are given below,

2.2.1. Chemical Methods

- Chemical techniques.
- Chemical vapor deposition.
- Vapor phase synthesis.
- Hydrothermal synthesis.
- Sonochemical techniques.
- Micro emulsion techniques.
- Wet chemical process.
- Sol-gel process.
- Co-precipitation method.

2.2.2. Physical Methods

- Laser ablation.
- Inert gas condensation.
- Spray route pyrolysis.
- Sputtering.

2.3. Synthesis of Maghemite Nanoparticles

I utilized sol-gel method for the synthesis of maghemite nanoparticles are described below.

2.3.1. Sol-gel Method

Sol-gel process is a very advantageous experimental technique for the preparation of γ-Fe_2O_3 nanoparticle. With the assistance of this technique one can synthesize nanomaterials from atoms/molecules. Products which are prepare by this method give high quality of crystallinity, narrow shapes distributions and are controlled [97]. For the preparation of γ-Fe_2O_3 nanoparticles following chemicals are used in proper ratio.

- Iron nitrate ($Fe(NO_3)_3.9H_2O$).
- Ethanol (C_2H_6O).
- Distilled water (H_2O).
- Citric acid ($C_6H_8O_7.H_2O$).

25

- Tetraethylorthosilicate (TEOS),
- Ammonia.

I started my process by the measurement of materials weight by using electronic weight balance. After this I put 10 g of Iron nitrate (Fe $(NO_3)_3.9H_2O$) and 20 ml of ethanol into a beaker and place this beaker on the magnetic stirrer for stirring to get homogeneous mixture than take second beaker and put 5.20 g of citric acid ($C_6H_8O_7.H_2O$) and 20 ml of distilled water and place this beaker on second some other magnetic stirrer for stirring function. That procedure is shown in Fig. 2.1.
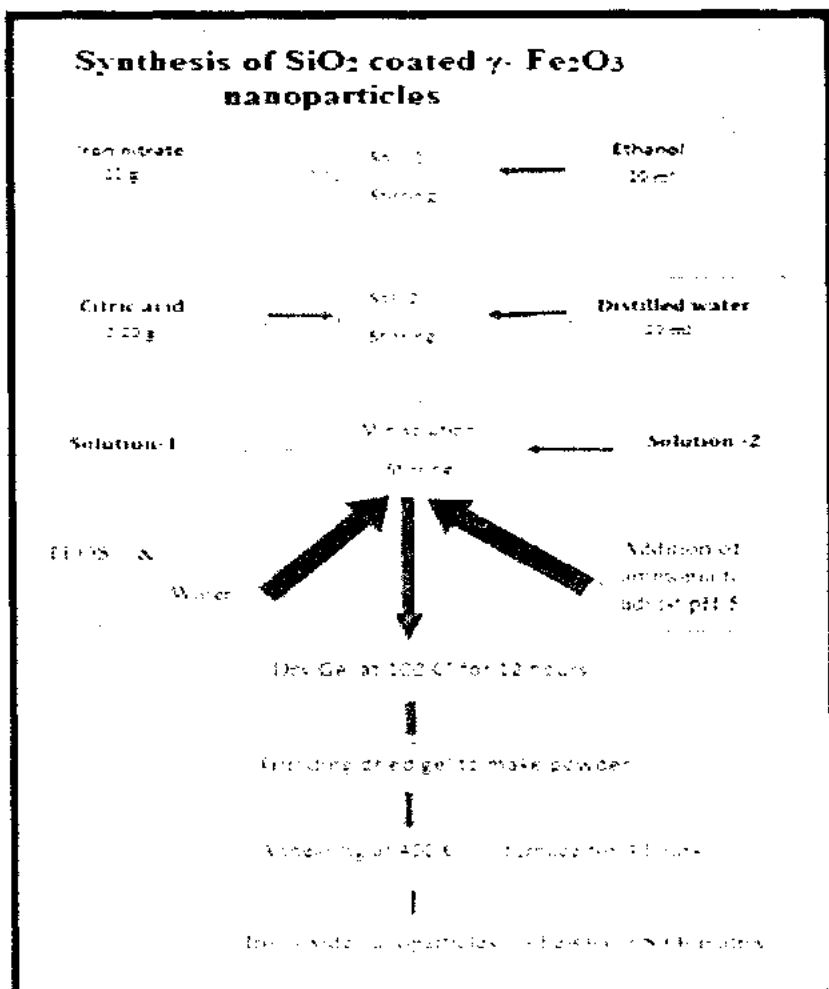
Fig. 2.1: Flow chart of synthesis process of SiO_2 coated γ-Fe_2O_3 nanoparticles.

After some time when I noticed homogeneous mixture is formed in both beakers, than I put the mixture of one beaker into the mixture of another beaker and place it on magnetic stirrer for stirring function to get regular and homogenous mixture. According to my requirement to get

26

the silica coated γ-Fe$_2$O$_3$ nanoparticle of 60 % weightage. I added 6.44 ml amount of TEOS (used as a precursor for SiO$_2$) and 2.088 ml amount of water into the mixture and left them for stirring for a while to attain the necessitated pH. I added ammonia drop by drop to get pH equal to 5 after obtaining this I put the heating button of magnetic stirrer for heating the mixture to get gel form. After a regular interval of time I checked the temperature which must be in its maximum limit of sample which is close to 80 °C. After a frame of time formation of gel started and we get mixture in gel form after some time. I stopped the process and place the beaker of gel at 100 °C for 12 h in microwave oven to evaporate water. After complete interval of time I took out the sample from microwave oven and is grinded by using mortar and pestle. When I get sample in fully powder like form than I annealed my sample in furnace for 4 h at 400 °C to get required phase. After the completion of time I take out the sample from furnace and grinded again than saved the sample in sample bottle.

CHAPTER 3

Characterization Techniques

We applied different characterization techniques for examining the samples like X-ray diffraction (XRD), scanning electron microscopy (SEM), Fourier transform infrared (FTIR), and superconducting quantum interference device (SQUID) magnetometer. Detailed working principles of all these techniques are described below.

3.1. X-ray Diffraction

Firstly in 1895, German physicist Roentgen discovered the x-rays. Due to its unknown nature he named them x-rays [98]. X-rays are electromagnetic radiations which are lying between gamma and ultra violet rays. These radiations can be produced by the collisions of fast accelerating electrons with metal target. These high accelerated electrons can be produced by heating the filament. For accelerating purpose these electron are passed through the porous cathode as described in Fig. 3.1.
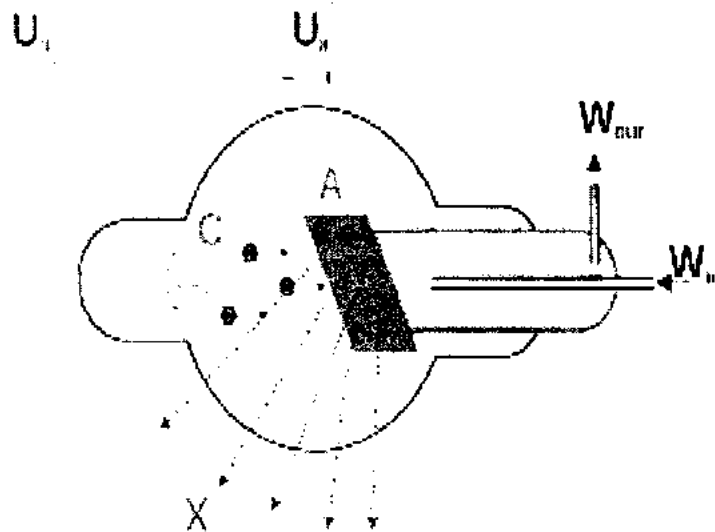
Fig. 3.1: X-rays production mechanism [99].

For the production of x-rays there must be source for electrons production. High voltage is needed for accelerating electrons and a target containing metal. X-ray diffraction (XRD) technique is used to identify the material. Information about chemical composition, crystal structure and physical properties of thin films. It works on diffraction and interference. The

interference could be constructive or destructive. For constructive interference, the size of inter-atomic spacing of the sample must be comparative to the wavelength of incident x-ray radiations [100,101]. There are mainly three factors which tune the reflected rays intensity, the incident X-rays wavelength, angle of incidence and their inter planer spacing. Diffraction is basically a scattering of incident x-rays from large numbers of atoms of the crystal. As in the crystal lattice the atoms are arranged in a specific periodic arrangements having specific geometry that's why there is a special phase relationship between the scattered rays and atoms arrangement. Destructive interference results no peak so it does not give any information. But when the constructive interference occur it give full information about the sample [98].

3.1.1. Bragg's Law

Bragg's derived a relation between incident wavelength, inter-planner spacing's and angle of incidence, which is known as Bragg's law. For X-rays to interfere constructively must satisfy the following condition as given bellow,

$$n\lambda = 2d \sin \theta \qquad (3.1)$$

Where "n" is an integer no., "λ" is wave length of incident x-ray, "d" is the inter-planer spacing and "θ" is scattering angle. Bragg's diffraction is shown in Fig. 3.2.
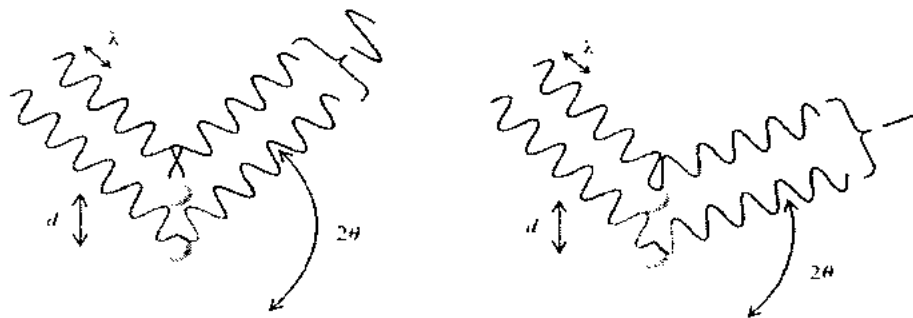
Fig. 3.2: Bragg's reflection [102].

3.2. Diffraction Methods

Bragg's law must be fulfilled for the occurrence of constructive diffraction. These parameters must be fixed to obtains diffraction by satisfying the Bragg's equation and can be tune during the experiment by changing the value of "λ" or "θ". On the basis of the arrangement of parameters there are three special methods for diffraction which are given below as.

- Laue method.

- Powder method.

- Rotating crystal method.

3.2.1. Laue Method

Laue method is used to find the orientation and nature of material [103]. In this method sample is kept fixed while the x-rays wavelength "λ" varied unless the Bragg's conditions satisfied to get constructive interference fixed as shown in Fig. 3.3.
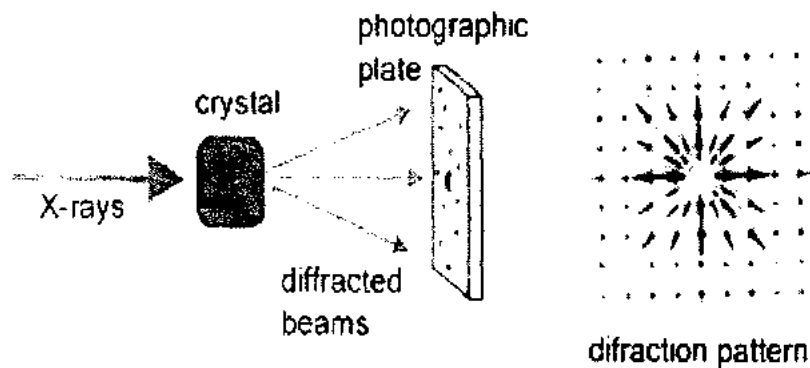
Fig. 3.3: Laue diffraction with varying diffracted wavelengths [104].

Hence for each set of planes the angle of incidence "θ" is fixed in Laue method. Diffraction occurs when Bragg's condition is satisfied by the specific value of wavelengths for fixed values of "d" and "θ". So each diffracted beam appears with a specific wavelength [98].

3.2.2. Powder Method

This method is used for the analysis of crystal structure. In this method a monochromatic beam of x-rays falls on the fine powder form sample. In the powder form every particle is oriented in an irregular arrangement in accordance with the incident x-ray beam so there are fewer chances that some of the particles will diffract the x-rays constructively. In this method every set of planes have ability to perform the phenomena of reflection [98]. The powder method is shown in Fig. 3.4.

(a)   (b)
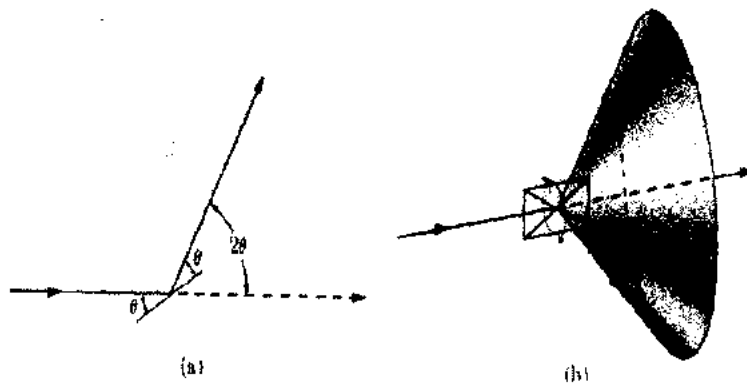
Fig. 3.4: Diffraction by powder method [105].

3.2.3. Rotating Crystal Method

Rotating crystal method is also used for study of crystal structure. In this method the wavelength of incident x-rays beam is kept constant and the incident angle is changed by rotating the sample. Crystal is put on along one of its axes or some particular crystallographic orientation. The monochromatic x-ray beam is falling perpendicular on the sample as shown in Fig. 3.5. A film which is in cylindrical structure is balanced around it and the crystal is permitted to rotate along the predefined direction. Both the axis (film axis and crystal axis) coinciding with each other. During the rotation process of crystal, specific set of planes satisfy the Bragg's law and reflection of monochromatic x-rays beam occurred [98].
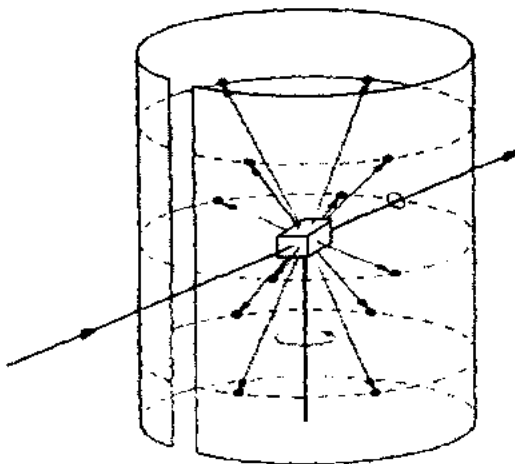
Fig. 3.5: Rotating crystal method [105]

31

3.2.4. Particle Size Determination

For the measurement of average particle size Debye Scherrer formula is used as given in Eq. (3.2). Paul Scherer introduced this formula. Limitations of its grain size measurement lies in range from 0.1 to 0.2 μm. Due to this Scherer's formula is comparatively better than Transmission electron microscope (TEM) which can measure particle size up to 5 %. [106].

$$D = \frac{0.9\lambda}{\beta \cos \theta_B} \qquad (3.2)$$

Where "β" represents the full width at half maximum (FWHM) which is shown in Fig. 3.6. It is measured in radians. Bragg's angle is symbolized by "θ_B" while crystallite's size is represented by "D". Diffraction curve width "β" has an inverse relation with thickness of crystal, i.e. when width of curve increases then the size of particle decreases.
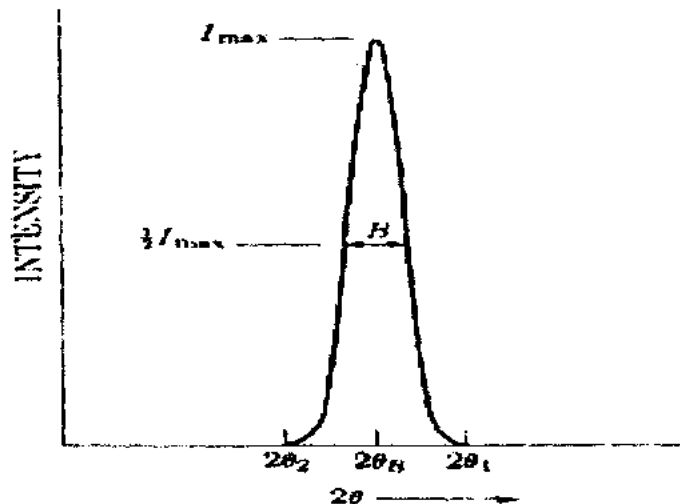
Fig. 3.6: FWHM diffraction curve [107].

The value of β can be obtained from the following relation.

$$\beta = \frac{1}{2}(2\theta_1 - 2\theta_2) \qquad (3.3)$$

3.3. Scanning Electron Microscopy

The scanning electron microscopy (SEM) is the widely used technique for detail study of the materials. It is used for examining morphological structure, particle size distribution, material surface and grain size analysis. The prominent advantage of SEM over x-rays diffraction is that it gives direct images of the materials. The main parts of scanning electron

microscopy are electron beam, scanning system, detectors, display monitor, vacuum system and electronics controls.

Working

SEM is based on emitted electron as photon in optical microscopy. In SEM, electrons beam is emitted from heated filament. To control the flow of electrons beam the electric field is used so that these electrons acquire enough kinetic energy. For maximum accuracy in results the electrons beam passed through series of electromagnetic lenses. In SEM, each specimen point that hit's by accelerated electrons produces signals in electromagnetic radiation from its selected part. Generally SE, BSE are collected by a detector and amplified and then showed computer monitor as shown in Fig. 3.7.
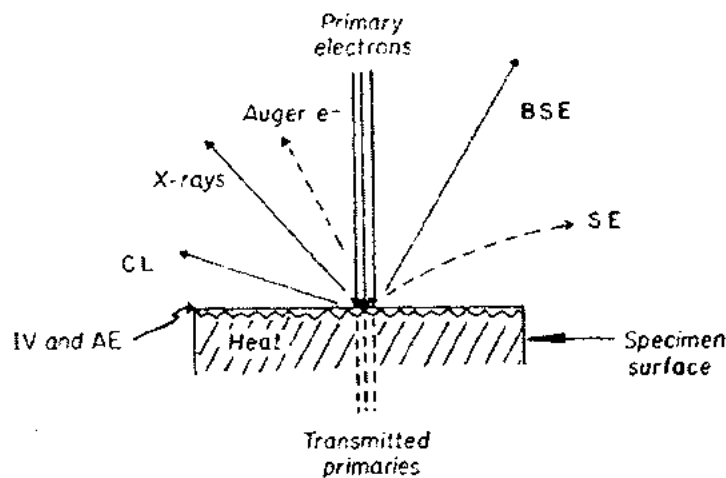
Fig. 3.7: Collection of radiation at detector [108].

When the electron beam interacts with sample it produces backscattered electrons, diffracted electrons, secondary electrons, heat, visible light and photons. The region where the incident electron beam interacts with the specimen is known as interaction volume. The backscattered and secondary electrons produce image of specimens which give useful information about specimen as shown in Fig. 3.8.

33
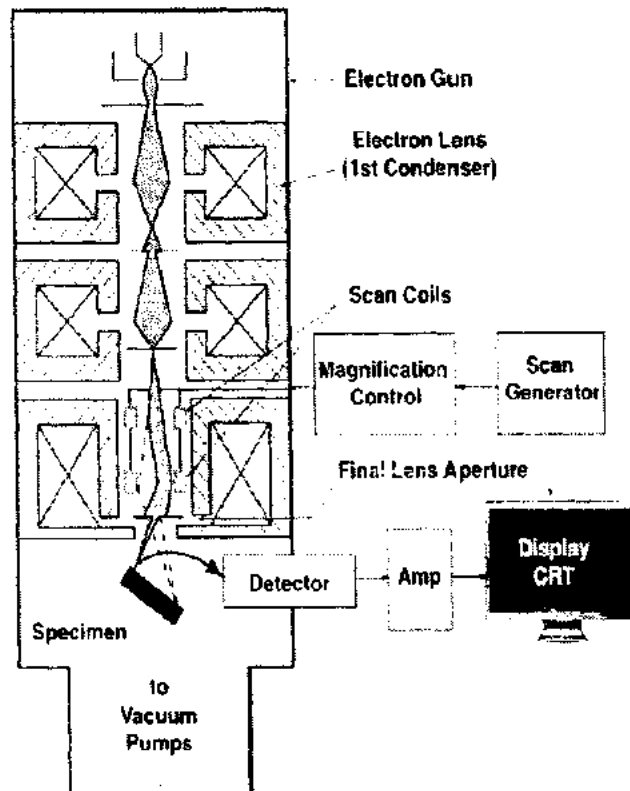
Fig. 3.8: Parts of SEM [108].

The image formed by SEM is a 2D intensity map in the digital or analog domain. In this every image pixel on display is proportional to the signal intensity captured by the detector at each specific point of the sample.

In scanning electron microscopy magnification entirely depends on the excitation of the scan coils and its numerical value is determined by that mathematical formula.

$$M = \frac{L_{mon}}{L_{spec}}$$ (3.4)

In which L_{mon} is the length of monitor and L_{spec} is length of the scan on the specimen.

3.4. Fourier Transform Infrared (FTIR) Spectroscopy

FTIR is a non-destructive technique used for the recognition of nature of unknown materials whether material is organic or in organic and. Its quality depends upon vibrations of atoms about their mean positions in materials. FTIR spectroscopy includes the absorption, emission, reflection and spectrum obtained by Fourier transform of an optical interferogram.

34

FTIR spectroscopy is used for a wide range of frequencies varying over ultraviolet, visible, far infrared, mid infrared, near infrared regions by selecting different detectors and beam splitters for the necessitated ranges. Other dispersive techniques are not capable for such a broad range of frequencies.

In FTIR, when sample is exposed by infrared radiations the transmission and absorptions of these infrared radiations measured the accompanying wavelengths of the infrared radiations and vibration of atoms about their mean positions gives data about separations among the atoms of material, chemical bonding between the atoms and nature of atom which is most necessary information. In this spectroscopy IR radiation passes from the sample a part of radiation is absorbed and part is transmitted so by combining the transmitting and absorbing infra-red radiation spectrum is obtained. FTIR lab apparatus as shown in Fig. 3.9.
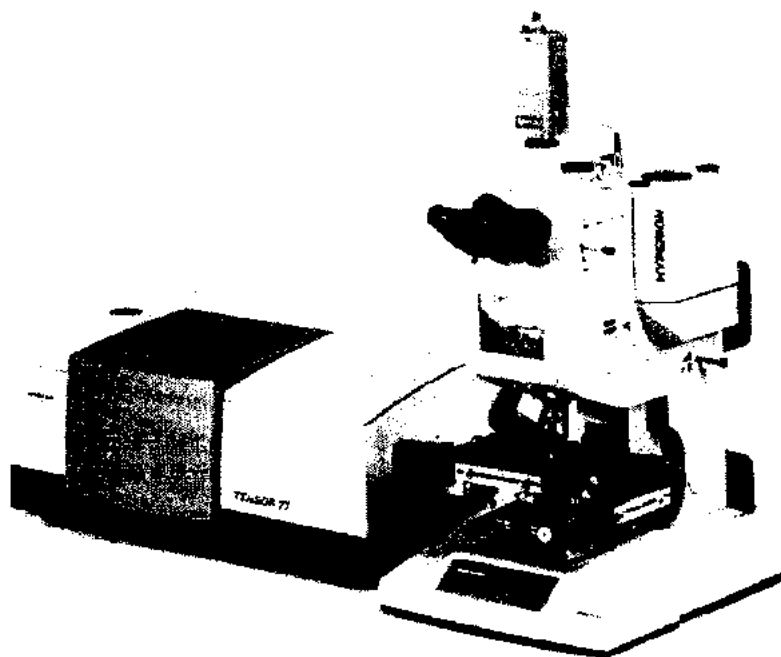
Fig. 3.9: Lab apparatus of Fourier transform infrared (FTIR) spectroscopy [109].

The Michelson interferometer is the most important part of infrared spectroscopy. It consists of Beam splitter, two mirrors and infrared detector. One mirror is fixed and other is moveable. Half portion of radiation is transmitted and remaining portion is reflected by fixed and moveable mirrors these infrared radiations recombine with each other and give rise to

interference before passed through detector for materials analysis. Michelson interferometer experimental arrangement is shown in Fig. 3.10.
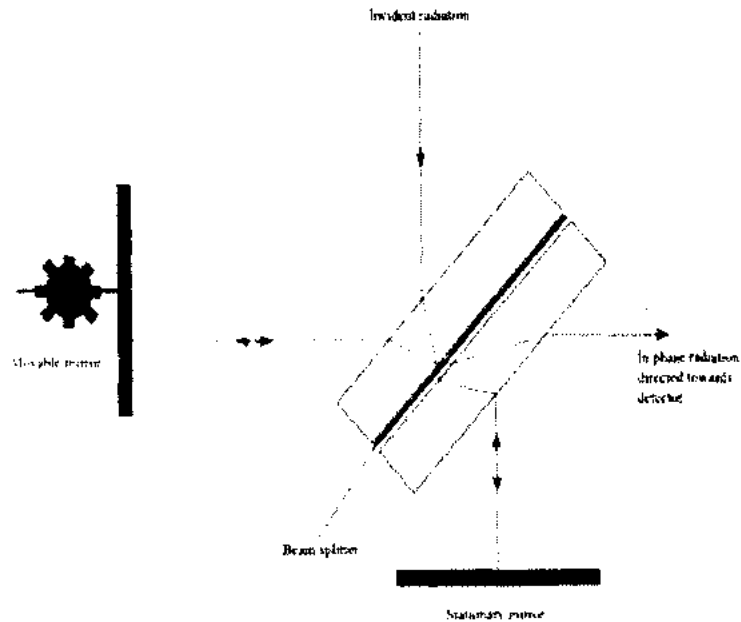
Fig. 3.10: Experimental arrangement of Michelson interferometer [110].

Beam splitter is a semi silvered glass plate which is semitransparent for radiations. It placed in such a way that it reflects and transmit half portion of infrared radiation. The reflected and transmitted light hits the fix and movable mirror accordingly. These radiations reflected back by mirrors and at beam splitter recombine with each other. If distance travelled by two beams of infrared radiation is the same that means distance between beam splitter and two mirrors is the same this state is defined as zero path difference (ZPD). If rotating mirror moves away from beam splitter means radiation covers longer distance which strikes with movable mirror comparing to radiation which strike with fix mirror. Mirror displacement is the distance which the movable mirror is away from ZPD and symbolized as Δ, so extra distance covered by radiation is represented as 2Δ. Extra distance is defined as optical path difference (OPD) and written as,

$$\delta = 2\Delta \qquad (3.5)$$

It is well established when optical path difference is the multiples of the wavelength than constructive interference takes place and due to this at detector maximum strength signals are observed which is reported by the following equation as,

36

$$\delta = n\lambda \qquad (n = 0,1,2,3,...) \qquad (3.6)$$

But when OPD is half wavelength add multiples of wavelengths than destructive interference takes place and due to this at detector minimum strength signals are observed which can be described by that equation,

$$\delta = (n + \tfrac{1}{2}\lambda) \qquad (n = 0,1,2,3,...) \qquad (3.7)$$

When OPD is between these than signal should be between minimum and maximum. The plot is known as an interferogram. Infrared detector is the instrument used to calculate the energy of infrared radiation. It is of two types' semiconductor and thermal detector [111]. Every sample can absorb different amount of radiation depending upon the strength of bonds and structure. When radiation enters into detector than detector produces signals. Because the measured interferogram signal cannot be directly understood that's why for decoding Fourier transformation a well-known mathematical technique is used and transformation is did by the computer as shown in Fig. 3.11.

| Interferograms | CPU | Spectrum |
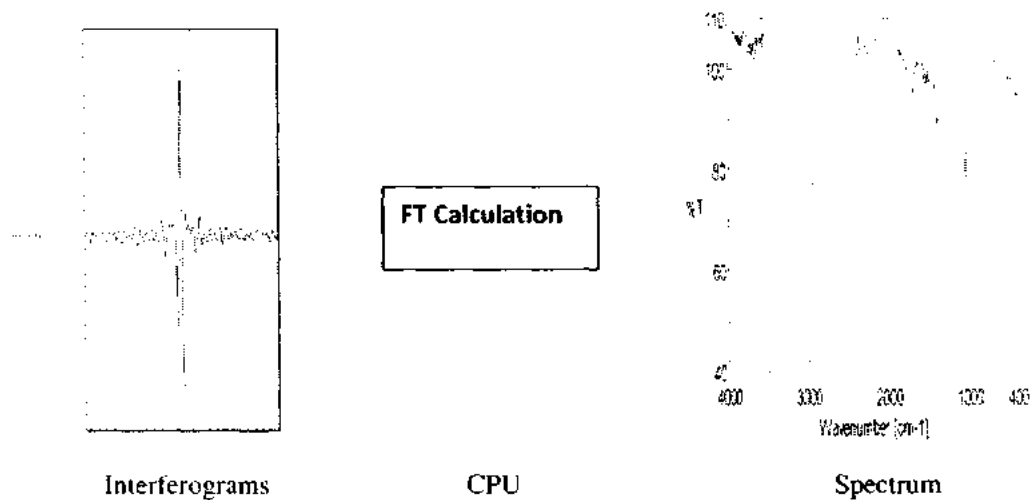
Fig. 3.11: Formation of FTIR spectrum [112].

3.5. Superconducting Quantum Interference Device Magnetometer

Superconducting quantum interference device is a highly sensitive magnetometer used for magnetic measurements and based on quantum effects in superconducting loop. This device is widely used in the field of medicine, biology and physics. In 1962, British physicist B.D

Josephson discovers Josephson Effect and on the base of this he invents Josephson junction. Superconducting quantum interference device contains a superconducting closed loop separated by a barrier (insulating tunnel barrier) having inner diameter of nearly 100 μm. There are one or two Josephson junctions in the path of loop known as weak links as shown in Fig. 3.12.

Voltage

Current

Current

Josephson junction
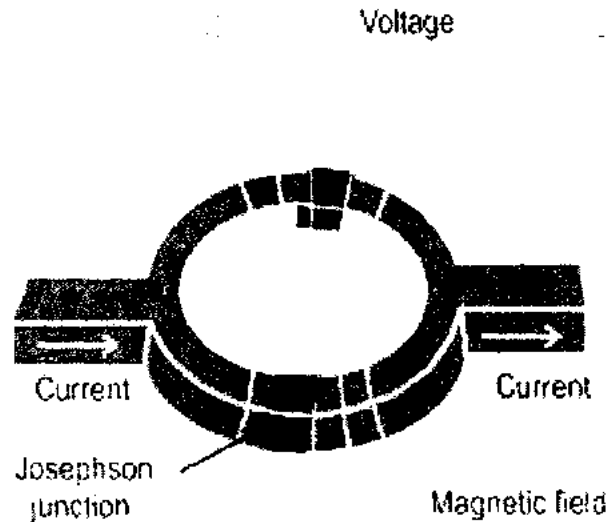
Magnetic field

Fig. 3.12: Josephson junctions [113].

Superconducting quantum interference device have the ability to work in larger fields approaching to 7 T and that can resolve the changes originated in external magnetic field up to 10^{-15} T because of superconducting ring having quantized state.

SQUID consists of a high-temperature superconductor (HTS) thin-film SQUID chip, two feedback coils to couple an external signal to the SQUID and to regulate it, magnetic shield, and a cable to connect the probe to the electronics box and superconducting detection coil and magnet.

Though SQUID is a highly sensitive device but it cannot measure magnetic field directly from the sample. A coil is used for the movement of the sample connected with Superconducting quantum interference device with the help of superconducting wires. Current from the detection coil is coupled with the SQUID through wires. Superconducting quantum interference device work as current to voltage converter and the output voltage is directly proportional to the current of input coil as shown in Fig. 3.13.

38
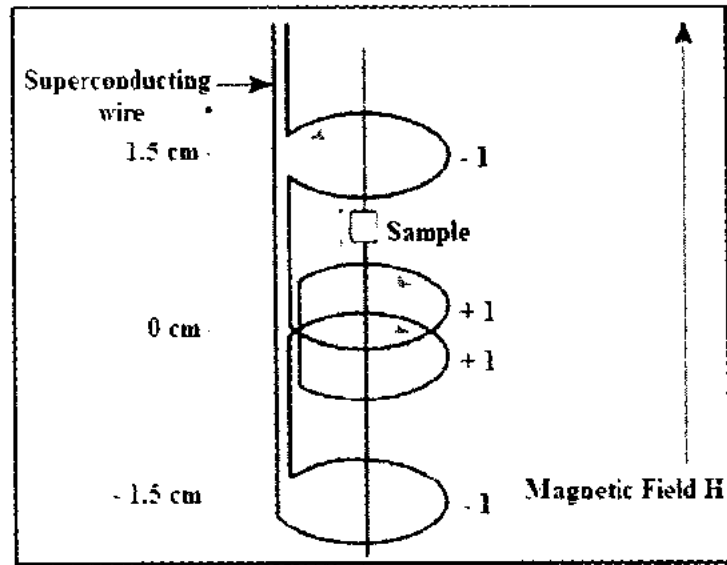
Fig. 3.13: Superconducting detection coil system in SQUID [114]

Magnetic property measurement system (MPMS) takes measurements only when detection coil moves the sample which is located at the magnet center and outside the chamber of a sample. A current is produced by the magnetic moments of a sample when sample is moved with the help of coils and these are act as detection coils. When magnetic flux changes then it give rise to a persistent current in detection circuit due superconducting closed loop.

CHAPTER 4

Results and Discussion

Spinel ferrites are the fascinating materials which attain the intention of researchers due to their promising potential applications in the field of industry such as, gas sensors, ferrofluids, and high density storage media. Structure of the nanoparticle, intrinsic and extrinsic properties can be controlled by different parameters such as synthesis methods, surface coating, reaction temperature and chemical composition. All spinel ferrites have vast range of applications but the preference of maghemite (γ-Fe_2O_3) over other ferrites is its chemical stability. Maghemite has the inverse spinel structure similar to magnetite with only Fe (II) deficiency. Formula unit of maghemite is $(Fe_8^{+3})_A[Fe_{40/3}^{+3}\Delta_{8/3}]_BO_{32}$, in which A and B represent tetrahedral and octahedral site and Δ represents vacancy at octahedral lattice site. The versatility of maghemite depends upon on the possibility of obtaining this material as particles of diverse morphologies. This finds interesting applications such as magnetic refrigeration, magnetic sensors, ferrofluids and information storage. In addition maghemite nanoparticle coated with bio ligands have variety of uses in bio separations and inmmunoassays and if particle is coated with silica it shows interesting magneto-optical properties and also used as a sensor for Earth's magnetic field. Maghemite (γ-Fe_2O_3) is also frequently used as a model to understand the magnetic properties of a ferromagnetic materials. Agglomeration is a big hurdle in order to study the properties of a material. The best way to avoid agglomeration is that magnetic particles are dispersed in a non-magnetic matrix. For this purpose I used SiO_2 to coat maghemite nanoparticles. For the study of structural and magnetic properties we used X-ray diffraction, scanning electron microscopy, Fourier transform infrared spectroscopy and superconducting quantum interference device magnetometer.

4.1. X-Ray Diffraction

X-ray diffraction is widely used technique for structural study and to compute the average crystallite size of the materials [115]. The crystalline structure of maghemite nanoparticles was characterized by X-ray diffraction (XRD, PHILIPS, XPert-MPD) utilizing Cu-Kα radiations of wavelength ($\lambda = 0.154$ nm) at the rate of 2°/min in the range of within the range of (20° – 70°). XRD diffractogram of SiO_2 coated maghemite nanoparticles is shown in Fig. 4.1. The indexed peaks (200), (311), (400), (422), (511) and (440) represent the miller indices of different diffraction planes at different angles $2\theta = 30°$, 35°, 43°, 53°, 58° and 63°, respectively for SiO_2

40

coated maghemite nanoparticles. These diffraction peaks are compatible with the maghemite (JCPDS card No: 39-1346) standard structure and confirms face-centered cubic inverse spinel structure of the sample. The effect of SiO_2 on the particle is the formation of Si–O–Si network during the synthesis of sample in which nucleation of the maghemite nanoparticles happens. As the concentration increases more nucleation centers formed which restricts the particle growth [116].
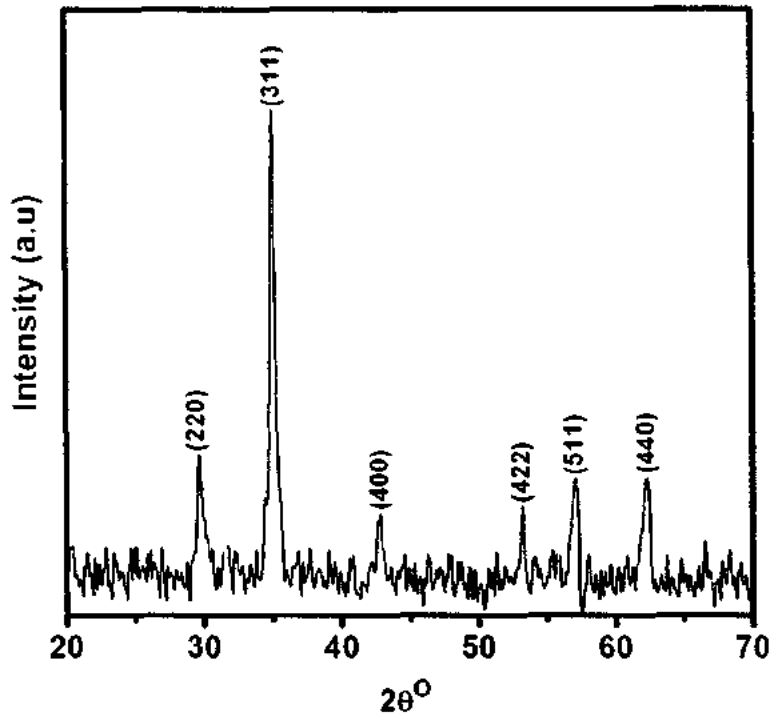
Fig. 4.1: XRD pattern of silica coated maghemite (γ-Fe$_2$O$_3$) nanoparticles.

The average crystallite size of the nanoparticles was calculated by using Debye Scherrer's formula, which is written in mathematical form as,

$$D = \frac{0.89\lambda}{\beta \cos \theta_B} \qquad (4.1)$$

In above eq. (4.1) D = average crystallite size, k= constant dependent on crystallite shape with value 0.91, λ = wavelength of XRD (λ = 0.15406 nm), θ = Braggs angle measured in radians, β= full width at half maximum of the XRD peak [117]. The calculated average crystallite size of maghemite nanoparticles is 19 nm. Due to amorphous nature of the SiO_2. XRD does not

41

uncovered any characteristic about SiO_2 but confirms the crystallinity of maghemite nanoparticles very well.

4.2. Scanning Electron Microscopy

SEM is the imaging technique used to examine the shapes and surface of materials whether it is at nano or bulk level and to estimate the particle size of them [118]. Surface morphology of maghemite nanoparticles is done with the assistance of SEM. Fig. 4.2 shows the image of maghemite nanoparticles coated with SiO_2 matrix (60 % wt. of total nitrates) at 200 nm scale and magnification X70. 000.
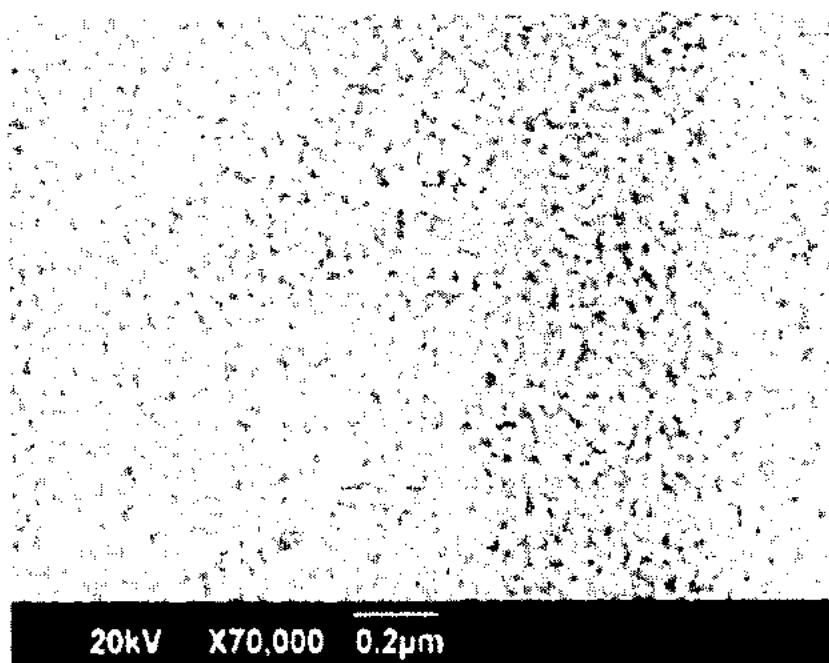
Fig. 4.2: SEM image of SiO_2 coated maghemite (γ-Fe_2O_3) nanoparticles at 200 nm scale and X70, 000.

From SEM micrograph it is observed that nanoparticles are about spherical in shape and have narrow particle size distribution. No agglomeration is seen which confirms the presence of amorphous SiO_2 that behave as a spacer between the particles.

4.3. Fourier Transform Infrared (FTIR) Spectroscopy

Fourier Transform Infrared (FTIR) Spectroscopy is a critical tool which is used to study the nature and chemical bonding between the material components. XRD technique does not give any information about the amorphous SiO_2 that's why we used FTIR to study and confirm

42

the formation of coating material SiO_2 on maghemite nanoparticles. Fig. 4.3 shows the FTIR spectrum of SiO_2 coated maghemite nanoparticle. It is observed that some maghemite bands e.g. bands at 440 and 480 cm⁻¹ are coincide partially with SiO_2 broad band at 470 cm⁻¹ and this band at 470 cm⁻¹ is the feature of Si-O-Si bending vibration. The separated maghemite bands from SiO_2 are at 693 and 553 cm⁻¹. The presence of Si-O-Fe vibrational band is at 953 cm⁻¹ which confirms the SiO_2 matrix and maghemite nanoparticles interaction. In addition asymmetric and symmetric Si-O-Si stretching vibration bands at 1097 and 815 cm⁻¹ are also noticed.
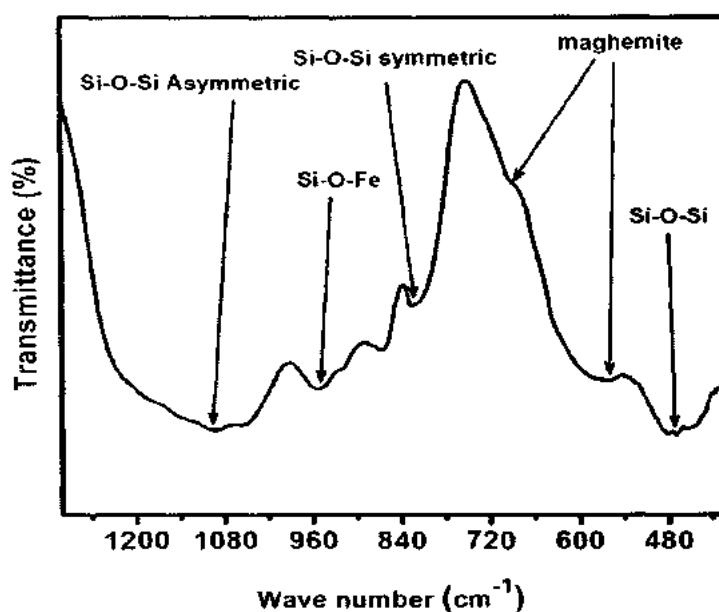
Fig. 4.3: FTIR spectrum of SiO_2 coated γ-Fe_2O_3 nanoparticles.

4.4. Zero Field Cooled and Field Cooled Magnetization

Magnetic measurements were done by utilizing a SQUID-magnetometer (Quantum Design, MPMS-XL-7) installed at Institute of Physics, Karl-Franzens University, Graz, Austria. Fig. 4.4 demonstrate the temperature dependent field cooled (FC) and zero field cooled (ZFC) curves of SiO_2 coated maghemite nanoparticles.
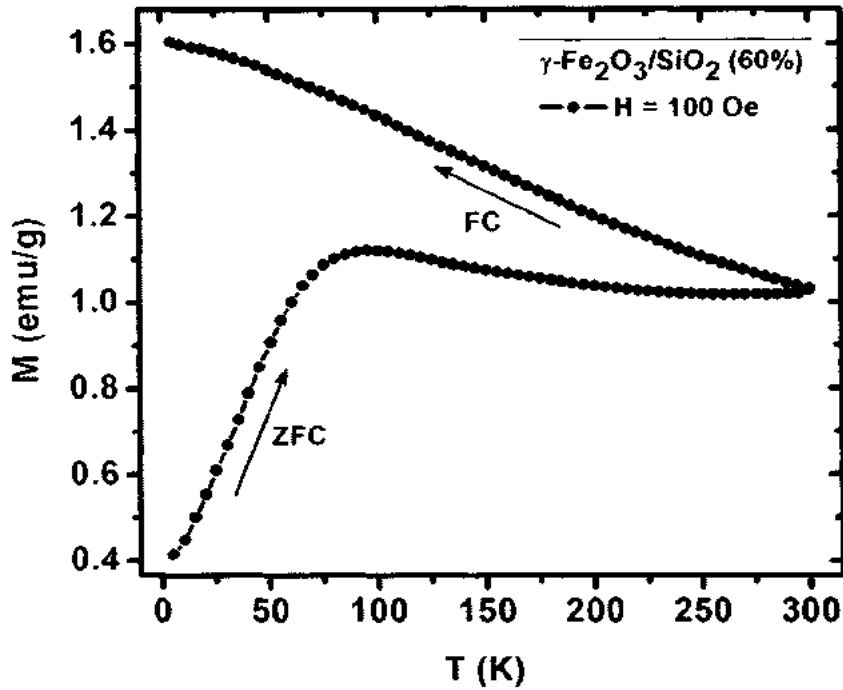
Fig. 4.4: FC and ZFC magnetization curves for SiO_2 coated γ-Fe_2O_3 nanoparticles.

For zero field cooled (ZFC) the nanoparticles were cooled down to 4.2 K in the absence of external field. At 4.2 K, magnetization is measured as per increasing the temperature in the presence of applied field (H) = 100 Oe. In ZFC, as temperature builds up the arrangement of magnetic moments along the field are brought on. On further increasing T, thermal energy gets over the anisotropy energy barrier and arbitrarily frozen magnetic moments are deblocked from their anisotropy axes. The maximum in ZFC corresponds to average blocking temperature (T_B) of the nanoparticles. This observed behavior can be explained by using Neel-Arrhenius relation.

$$\tau = \tau_0 exp(\frac{E_A}{k_B T})$$ (4.2)

In above Eq. 4.2. $k_B T$ = thermal energy, E_A = anisotropy energy barrier and τ_0 is the atomic spin-flip time [119,120]. Here $E_A = K_{eff} V$ in which "V" is average volume of particle and "K_{eff}" is effective anisotropy constant. In order to reverse the magnetization of magnetic nanoparticle the huge core spin must exceed anisotropy energy barrier (E_A) of nanoparticle. This is possible only when the thermal energy is greater than anisotropy energy barrier. At

44

$k_BT> E_A$ the thermal energy is enough to deblock spins from their anisotropy direction and lastly they attain the superparamagnetic state [121]. The deblocked nanoparticle's huge core spin alters its magnetization direction many times during the estimation time and act as paramagnetic atom. Due to deblocked core spins magnetization decreases as the temperature increases and the higher external applied magnetic field has no such power to align these core spins. But at the condition $k_BT< E_A$, the thermal energy is not enough to surpass the anisotropy energy barrier that's why it can't deblock the nanoparticles huge core spins from their anisotropy axis. At that point the external applied strong magnetic field align the core spins.

Arrangement of magnetic moments along the field continues expanding up to T_B of the nanoparticles and after that moments show decreasing trend because of increase in thermal energy is now more than anisotropy energy barrier. At that condition the nanoparticles move to superparamagnetic state $(T > T_B)$ from blocked frozen state. Lower magnetization of ZFC curve at low temperatures is due to the randomly frozen nanoparticles spins. However, the M continuously increases with decreasing "T" which is due to applied field. In FC curve, the nanoparticles spins are not randomly blocked in their anisotropy axes due to presence of applied field which causes increase in "M" with decreasing "T". The continuous increase in "M" with decreasing "T" in FC curve at low temperatures is an indication of presence of lesser dipolar interactions among nanoparticles due to presence of amorphous non-magnetic SiO_2 surface coating. The SiO_2 acts as spacer between the particles to avoid agglomeration.

4.5. Temperature Dependent M-H Loops

M-H loops at 5 T field cooled (FC) for SiO_2 coated maghemite nanoparticle at different temperatures such as T= 5, 25, 50, 75, 100, 150, and 300 K are measured. It is observed that the M-H loops are not saturated even at ± 5 T. The saturation magnetization (M_s) increases with decreasing T. The "M_s" at 5 K comes out to be 24 emu/g which is much lower than the "M_s" value for bulk maghemite "M_s" (bulk) = 80 emu/g. The "M_s" value is strongly size dependent and decreases with decreasing particle size for ferrite nanoparticles [122]. The surface spin-glass freezing in ferrites and presence of SiO_2 matrix are the two main factors that are greatly responsible for the reduction of "M_s" in coated ferrite nanoparticles. Normally the surface spins have bond with core spins only on inner side. But as the silica coating has interaction with particle's surface that can also change the surface magnetization. Therefore silica coating has the significant effects on the magnetization reversal in maghemite nanoparticles [119]. M-H loops are shown in Fig. 4.5.
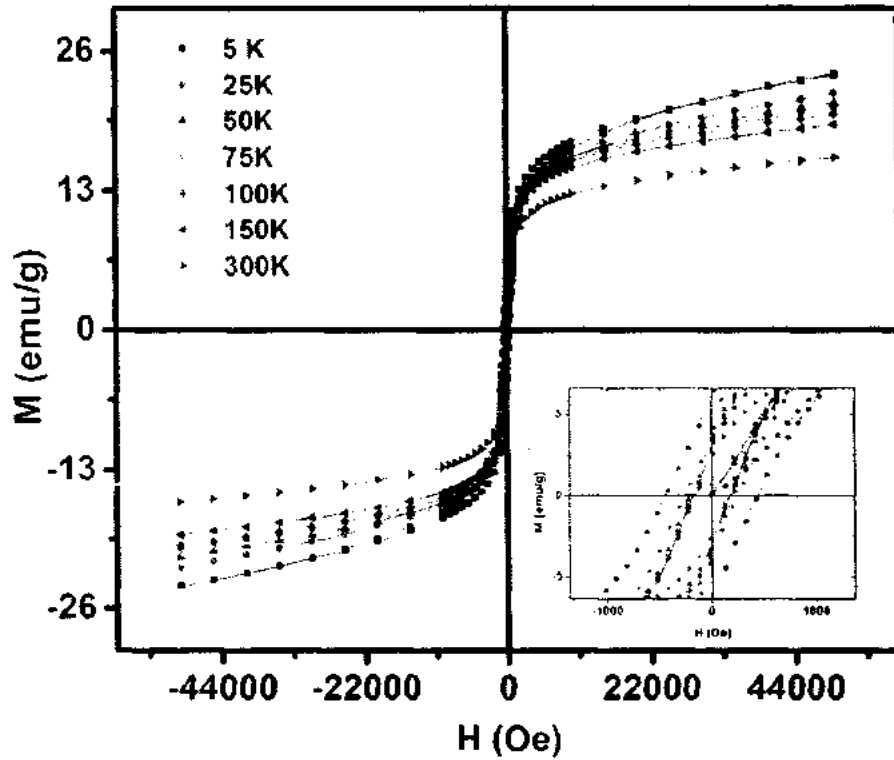
Fig. 4.5: M-H loops of SiO₂ coated γ-Fe₂O₃ nanoparticles at different temperatures. Inset represents the detailed behavior of the coercivity.

4.6. Temperature Dependent Saturation Magnetization

The "M₅" value strongly dependent upon temperature and decreases with increasing temperature [122]. The temperature dependent magnetization of SiO_2 coated nanoparticles at maximum applied field of ± 5 T is shown in Fig. 4.6 (a). The "M₅" value exhibits monotonous behavior, i.e. increases with decreasing temperature due to excitation of spin waves.

The temperature dependent "M₅" of nanoparticles can also examined by using Bloch's law [123]. Through this law it is observed that "M₅" consistently increases with decreasing temperature and that shows good fitting of Bloch's law as shown in Fig. 4.6 (b) [124].

Mathematically the Bloch's law can be written as,

$$M_s(T) = M_{so}(1 - BT^b) \qquad (4.3)$$

In this eq. b = Bloch exponent. B = Bloch constant, M_{so} = saturation magnetization value at 0 K and M_s (T) is the measured temperature dependent saturation magnetization. "B" and "b" are the fitting parameters [125].

46
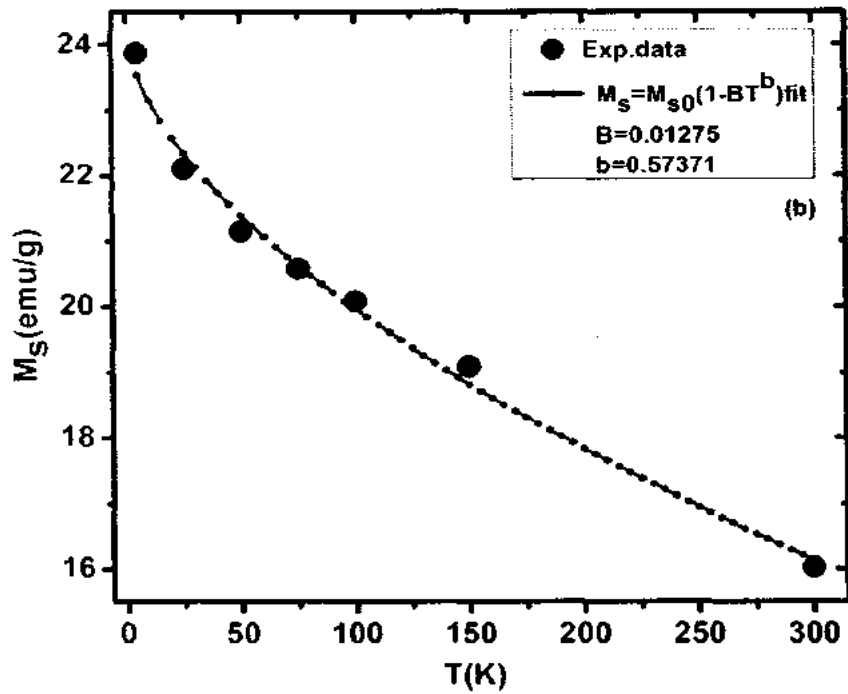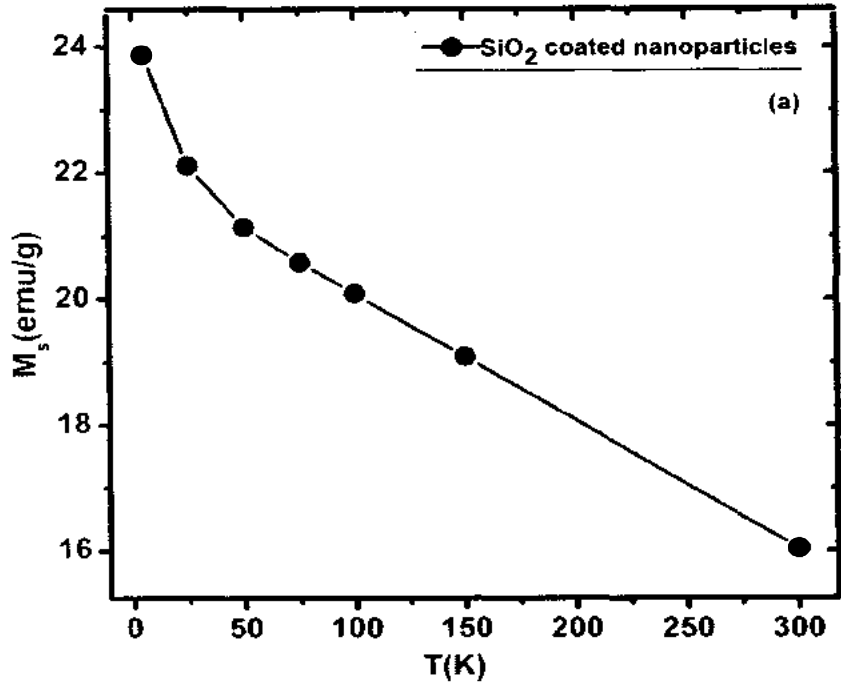
Fig. 4.6: (a) Temperature dependence saturation magnetization (M$_s$) for SiO$_2$ coated γ-Fe$_2$O$_3$ nanoparticles and

(b) Bloch's law fit (dot line) using Eq. (4.3) for SiO$_2$ coated γ-Fe$_2$O$_3$ nanoparticles.

Bloch's law fitting gives B = 0.01275 and b = 0.57371 for SiO₂ coated γ-Fe₂O₃ nanoparticles. Bloch's law demonstrates good fitting for SiO₂ coated γ-Fe₂O₃ nanoparticles. However the value of b is much lower than the value for 3 D systems such as 3/2.

4.7. Temperature Dependent Coercivity

Fig. 4.7 demonstrates the temperature dependence of coercivity (H$_c$) for SiO₂ coated γ-Fe₂O₃ nanoparticles.
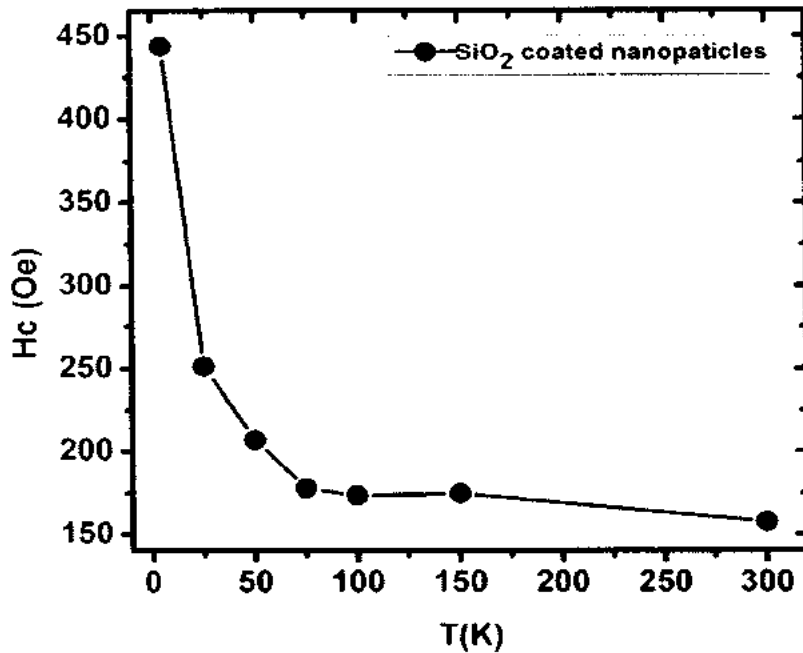
Fig. 4.7: Temperature dependence of coercivity (H$_c$) for SiO₂ coated γ-Fe₂O₃ nanoparticles.

It is observed that coercivity (H$_c$) shows a sharp increasing pattern at low temperatures which is attributed to the contribution of surface anisotropy (frozen surface spins) [126]. Coercivity of the coated nanoparticles increases monotonically with decreasing temperature due to reduction of thermal fluctuation of blocked moments across the anisotropy barrier [127]. At low temperatures, the anisotropy is the massive function of temperature for nanoparticles. Therefore "H$_c$" increases sharply due to contribution of strong surface anisotropy in them. Instead of anisotropy, the other factors such as structural properties, volume distributions, and inter-particle interactions are also effect the coercivity of the nanoparticles.

4.8. Temperature Dependent Remanent Magnetization

Fig. 4.8 shows the temperature dependence of remanent magnetization (M_r) for SiO_2 coated γ-Fe_2O_3 nanoparticles.
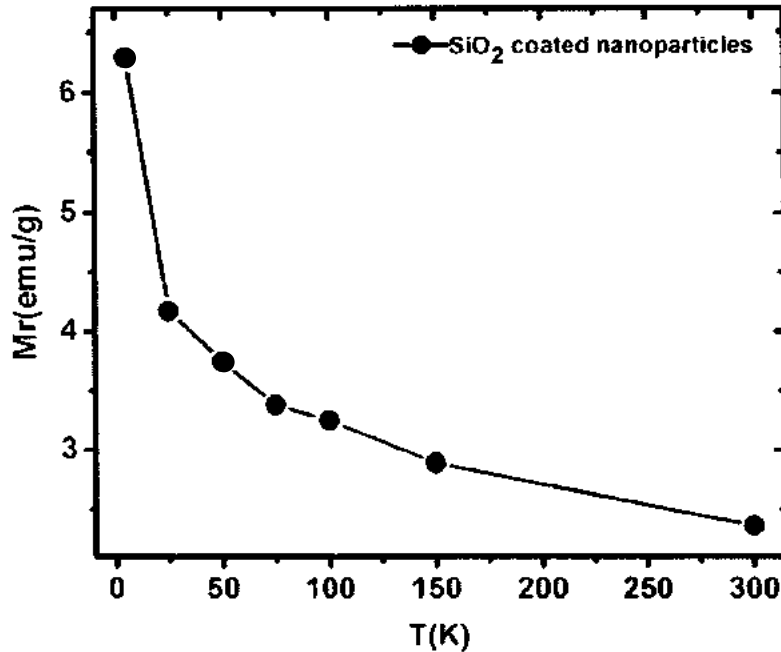
Fig. 4.8: Temperature dependence of remanent magnetization (M_r) for SiO_2 coated γ-Fe_2O_3 nanoparticles.

From figure increasing trend of remanent magnetization (M_r) at low temperatures is observed. Moreover step-like behavior near remanent field is also noticed. Both are credited to less dipolar interaction in coated nanoparticles [128]. Lower values of remanent magnetization ensures the soft magnetic nature of SiO_2 coated γ-Fe_2O_3 nanoparticles.

4.9. Magnetization Relaxation and Stretched Exponential Law Fit

We have done field cooled (FC) and zero field cooled (ZFC) magnetization for SiO_2 coated γ-Fe_2O_3 nanoparticles to study effects of SiO_2 coating on their relaxation dynamics.

4.9.1. Field Cooled Magnetic Relaxation

Fig. 4.9 shows the FC relaxation of magnetization (solid cubes) and stretched exponential law fit (line) for SiO_2 coated γ-Fe_2O_3 nanoparticles at temperature (T) = 5 K. For FC relaxation, the sample is first FC in 100 Oe from room temperature to target temperature (5 K). Afterwards the field is switched off and magnetization is recorded with time. It is interesting to note that

at low temperatures, the magnetization does not relax after switching off the field and continuously decreasing, which indicates the presence of slow spin dynamics or spin-glass in these coated nanoparticles [129].

Fig. 4.9: Field cooled magnetic relaxation (solid cubes) and stretched exponential law fit (−line) using Eq. (4.4) for SiO_2 coated γ-Fe_2O_3 nanoparticles.

Usually there are two models used to fit the relaxation data; (i) logarithmic relaxation decay model and (ii) stretched exponential decay model [130]. We have fitted relaxation curves of the relaxation curve recorded at 5 K using stretched exponential law as,

$$M = M_2 + (M_1 - M_2)\,exp(-(t/\tau)^\beta \qquad (4.4)$$

where M_1 and M_2 are initial and final magnetization. τ is the mean relaxation time and β is a shape parameter. "τ" and "β" are the fitting parameters. The initial parameters measured values at T= 5 K for fitting are M_1 = 0.73 and M_2 = 0.436. Obtained fitting parameters values are τ = 866 s and β = 0.45825. Exponential law shows good fitting on this data. The shape parameter (β) lies between 0 and 1 for different disordered systems. Spin-glass systems usually exhibit β in the range 0.2 − 0.6, below the freezing temperature [131]. Reported the β value equal to 0.52 for the spin-glass alloy La-Fe-Mn-Si, below freezing temperature. The long relaxation time and value of β indicates the presence of slow spin relaxation or spin-glass in SiO_2 coated nanoparticles. The slow relaxation of coated nanoparticles is due to their stronger spin-glass

behavior and interactions with the SiO_2 coating. In spin-glass systems, there are landscapes of irregular energy barriers and magnetic spins (in our case it is huge core spin of the nanoparticle) are trapped in them and requires more time for spin-flop. The longer spin-flip time is responsible for longer magnetic relaxation time.

4.9.2. Zero Field Cooled Magnetic Relaxation

Superparamagnetic systems show slow spin relaxation in the FC protocol only, while spin-glass systems show slow dynamics in both ZFC and FC protocols [132]. Therefore we have also investigated magnetic relaxation in ZFC protocol at 5 K (solid circles) and stretched exponential law fit (line) as shown in Fig. 4.10.
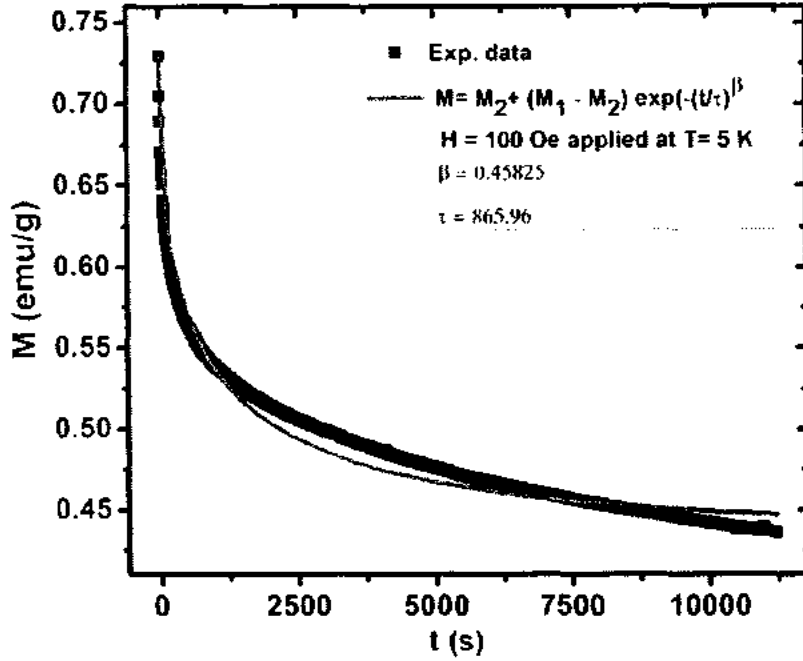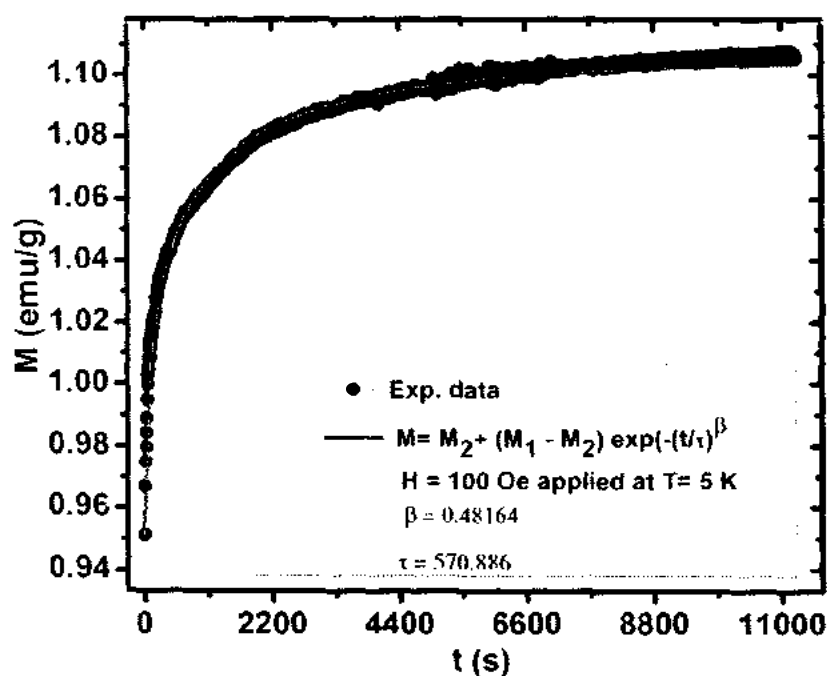

Fig. 4.10: Zero field cooled magnetic relaxation (solid spheres) and stretched exponential law fit (−line) using Eq. (4.4) for SiO_2 coated γ-Fe_2O_3 nanoparticles.

For ZFC relaxation, the sample was first ZFC to 5 K and then 100 Oe field is applied and magnetization is recorded with time. It is evident that the system also shows slow spin relaxation in ZFC protocol in addition to the FC protocol. Therefore our system shows slow spin relaxation in both FC and ZFC protocols which suggests the presence of spin-glass behavior. The initial parameters values for the fitting at T = 5 K are M_1 = 0.951 and M_2 = 1.1057. Obtained fitting parameters values are τ = 571 s and β = 0.48.

Conclusions

SiO$_2$ coated γ-Fe$_2$O$_3$ nanoparticles have been synthesized successfully by using sol-gel method. XRD reveals FCC inverse spinel structure for coated γ-Fe$_2$O$_3$ nanoparticles. The average crystallite size comes out to be 19 nm because large concentration of SiO$_2$ during growth restrict the particle size. The spherical shape of nanoparticles is confirmed by scanning electron microscope (SEM). Magnetic measurements show that hysteresis loops for coated maghemite nanoparticles are not saturated even at a low temperature due to presence of disordered surface spins which require rather high applied fields for saturation. The saturation magnetization is also drastically reduces for coated nanoparticles as compared to counter bulk maghemite due to large surface spin disorder, smaller crystallite size of nanoparticles and presence of non-magnetic SiO$_2$ coating material. The average blocking temperature (T$_B$) of maghemite nanoparticles is found to be lower than room temperature which shows their superparamagnetic nature at room temperature. The coercivity increases sharply at lower temperatures due to presence of stronger surface anisotropy contribution in them. Magnetic relaxation data shows the slow spin dynamics in both FC and ZFC protocols, which ensures the presence of spin-glass behavior in these SiO$_2$ coated γ-Fe$_2$O$_3$ nanoparticles. In summary, silica coated nanoparticles show stronger surface spins disorder and spin-glass behavior.

References

[1]. H. E. Schaefer, "Nanoscience" Springer, Berlin (2010).

[2]. G. A. Mansoori, "Principles of nanotechnology", World Scientific Publishing Co. Pte. Ltd. Singapore (2005).

[3]. E. Bichoutskaia, "Computational Nanoscience", RSC Publishing, Cambridge, UK (2011).

[4] P. Moriarty, Rep. Prog. Phys. **64**, 297 (2001).

[5] C. L. Peterson, IEEE Technology and Society Magazine (2004).

[6] J. Langwith, "Nanotechnology", Greenhaven Press, Detroit, MI (2009).

[7] V. Kumar, A. Rana, M. S. Yada. and R. P. Pant, J. Mang. Mang. Mater. **320**, 1729 (2008).

[8] C. Q. Sun, B. K. Tay, S. Li, X. W. Sun, S. P. Lau, and T. P. Chen, Mater. Phys. Mech. **4**, 129 (2001).

[9] M. V. Zelkowitz, "Nanotechnology" Elsevier Academic Press, Amsterdam (2007).

[10] A. Gadkari, T. Shinde, and P. Vasambekar, J. Mater. Sci. Mater. Electron. **21**, 96 (2010).

[11] R. Bhattacharya, and P. Mukherjee, Adv. Drug Deliv. Rev. **11**, 1289 (2008).

[12] W. Caseri, Macromol. Rapid Commun. **21**, 705 (2000).

[13] S. A. Yousaf, and S. Ali, J. Faculty Eng. & Technol. **11**, 20 (2008).

[14] J. Ramsden, "Essentials of Nanotechnology", BoBoCoAe, JR & Ventus Publishing APS (2009).

[15] E. Ebad, Nano dictionary (2005).

[16] R. P. Feynman, "There is Plenty of Room at the Bottom", California Institute of Technology (1959).

[17] T. C. Erren, Med. Hypotheses **68**, 732 (2007).

[18] J. Wilsdon, "The politics of small things: Nanotechnology, risk, and Uncertainty" IEEE (2004).

[19] BS PAS 71: Vocabulary. Nanoparticles. British Standard Institution (BSI), UK (2005).

[20] S. P. Leary. C. Y. Liu, C. Yu, and M. L. Apuzzo, Neurosurg 57, 606 (2005).

[21] S. Gelperina. K. Kisich, M. D. Iseman, and L. Heifets, Am. J. Respir. Crit. Care Med. 172, 1487 (2005).

[22] Z. Guo, and L. Tan. "Fundamentals and applications of nanomaterials". Artech house, Boston (2009).

[23] J. M. D. Coey, "Magnetism and Magnetic Materials", Cambridge University Press (2010).

[24] D. J. Griffiths. "Introduction to Electrodynamics", 3rd edition, Addison Wesley (1999).

[25] B. D. Cullity. and C. D. Graham, "Magnetic Anisotropy, in Introduction to Magnetic Materials", 2nd edition, John Wiley & Sons, Inc., Hoboken, NJ, USA (2008).

[26] Stöhr. Joachim, Siegmann, and H. Christoph, "Magnetism from Fundamentals to Nanoscale Dynamics", Springer series in Solid-State Sciences, Springer, Heidelberg (2006).

[27] S. L. Kakani and A. Kakani, "Material Science", New Age International (P) Ltd. Publishers (2004).

[28] H. J. Lipkin, and M. Peshkin, "Magnetic Monopoles and Dipoles in Quantum Mechanics", Argonne National Lab, Argonne, Ill (1986).

[29] https://www.physicsforums.com/threads/spin-magnetic-moment.773970/

[30] H. Li. E. Buns. K. Bears. Q. Ji, J. J. Lesko, D. A. Dillard, J. S. Riffle. and P. M. Puckett, J. Compos. Mater. 34, 1512 (2000).

[31] I. Dorfman. "Diamagnetism and the Chemical Bond". American Elsevier Pub, New York (1965).

[32] L. N. Mulay, "Magnetic Susceptibility" Interscience Publishers, New York (1966).

[33] www.csus.edu/indiv/n/ngw/EEE-161/wk-12/Lecture/Applied%20magnetism.ppt

[34] X. Gabriel, and E.Louis. "Paramagnetism. Diamagnetism", Hermann & Cie. Paris (1937).

[35] G. Cao, "Nanostructures and Nanomaterials – synthesis, Properties and application", Imperial College Press, London (2003)

[36] A. H. Morrish, "The Physical Principle of Magnetism", IEEE Press, New York (2001).

[37] E. Burts, "Dissertation", Virginia Tech, Blacksburg (2000).

[38] B. M. Moskowitz, "Hitchhiker's Guide to Magnetism", Elsevier Science (1991).

[39] R. M. Bozorth, "Ferromagnetism", Van Nostrand, New York (1951).

[40] D. K. Cheng, "Field and Wave Electrodynamics", 2nd edition, Addison Wesley Publishing Company (1983).

[41] E. D. Seifer, "Bosons, Ferromagnetism and Crystal Growth Research" Nova Science Publishers, New York (2007).

[42] C. Kittle, "Introduction to Solid State Physics", 8th edition, John Wiley and Sons (2005).

[43] T. Moriya, "Nuclear Magnetic Relaxation near the Curie Temperature", University of Tokyo, The Institute for Solid State Physics, Tokyo (1962).

[44] V. Michev, and K. Naoum, Phys. Rev. B **80**, 68 (2015).

[45] D. S. Mathew, and R. S. Juang, Chem. Eng. J. **29**, 51 (2007).

[46] E. W. Gorter, Nature **165**, 798 (1950).

[47] N. A. Spaldin, "Magnetic Materials: Fundamentals and Device Applications", Cambridge University Press (2013).

[48] http://www.mdpi.com/2075-163X/4/1/89/htm

[49] Z. Niu, and F. Li, Physica B **463**, 15 (2015).

[50] C. B. Neel, "An Investigation Utilizing an Electrical Analogue of Cyclic De-icing of a Hollow Steel Propeller with an External Blade Shoe", National Advisory Committee for Aeronautics, Washington, D.C (1952).

[51] A. Kumar, "Introduction to Solid State Physics", PHI Learning Pvt. Ltd. (2010).

[52] J. Lesko, and J. Florio, J. Adv. Mater. **28**, 55 (1997).

[53] G. H. O. Daalderop, "Magnetic Anisotropy from First Principles", S. n., S. 1 (1991).

[54] ASTM, "Annul Book of ASTM Standards", ASTM, West Conshohocken (1995).

[55] C. M. Sorensen, "Nanoscale Materials in Chemistry", A John Wiley & Sons, Inc., Publication, New York, (2001).

[56] R. H. Kodama, and A. E. Berkowitz, Phys. Rev. 59, 6321 (1999).

[57] M. Ozaki, "In Fine Particles: Synthesis. Characterization. and Mechanisms of Growth", Marcel Dekker, Inc., New York (2000).

[58] R. H. Kodama, J. Magn. Magn. Mater. 200, 359 (1999).

[59] K. L. Pisane. E. C. Despeaux, and M. S. Seehra. J. Magn. Magn. Mater. 384, 148 (2015).

[60] C. Kittel, "Introduction to Solid State Physics". A John Wiley & Sons, Inc., Publication. New York (1976).

[61] R. Kotitz, P. C. Fannin, and L. Trahms, J. Magn. Magn. Mater. 149, 42 (1995).

[62] J. G. Lee. J. Y. Park. and C. S. Kam, J. Mater. Sci. 33. 3965 (1998).

[63] E. C. Snelling. "Soft Ferrites: Properties and Applications", Iliffe, London (1969).

[64] G. Wulfsberg, "Inorganic Chemistry", University Science Books (2000).

[65] S. Son. M. Taheri. E. Carpenter, V. G. Harris. and M. E. McHenery, J. Appl. Phys. 91. 7589 (2002).

[66] K. Woo, J. Hong, S. Choi, H. Lee, J. Ahn, C. S. Kim. and S. W. Lee, Chem. Mater. 16, 2814 (2004).

[67] M. Faraji, Y. Yamini, and M. Rezaee, J. Iran. Chem. Soc. 7, 37 (2010).

[68] N. D. Kandpal, N. Sah, and R. joshi, J. Sci. Ind. Res. 73. 87 (2014).

[69] S. Laurent. D. Forge, Chem. Rev. 108. 2064 (2008).

[70] J. F. Liu. Z. S. Zhao. and G. B. Jiang, Environ. Sci. Technol. 42, 6949 (2008).

[71] R. M. Cornell, and U. Schwertmann, "The Iron Oxides. Structure, Properties, Reactions, Occurrence and Uses" VCH, Weinheim; Germany (1996).

[72] E. Matijević, and R. S. Sapieszko, "Force Hydrolysis in Homogeneous Solution: in Fine Particles: Synthesis, Characterization and Mechanism of Growth", Surfactant Science Series Marcel Dekker, Inc. **92**, 34 (2000).

[73] E. Matijević, "Fine particles: Science and Technology" MRS Bulletin (1989).

[74] A. H. Morrish, and K. Haneda, J. Appl. Phys. **63**, 2496 (1981).

[75] R. M. Cornell, and U. Schwertmann, "The Iron Oxides: Structure, Properties, Reactions, Occurrences and Uses" John Wiley & Sons, Inc. (2006).

[76] R. Dronskowski, Adv. Funct. Mater. **11**, 27 (2001).

[77] R. S. Tebble, and D. J. Craik, "Magnetic Materials", Wiley-Interscience, London (1969).

[78] R. M. Cornell, and U. Schertmann, "The Iron Oxides: Structure, Properties, Reactions, Occurrence and Uses", VCH Publishers, Weinheim (1996).

[79] L. C. Cullity, "Introduction to Magnetic Materials" Addison-Wesley Publishing Company. USA (1972).

[80] S. Laurent, D. Forge, M. Port, A. Roch. and C. Robic, Chem. Rev. **108(6)**, 2064(2008).

[81] M. Arruebo, and R. Ibarra, Drug Dev. Res. **2**, 22 (2007).

[82] C. J. Serna. and M. P. Morales, "Maghemite (γ-Fe2O3): A Versatile Magnetic Colloidal Material". Surface and Colloid Science. Springer. US (2004).

[83] M. Tadic. S. Krali. M. Jagodic, D. Hanzel. and D. Makovec, Appl. Surf. Sci. **322**, 255 (2014).

[84] A. Tsoukatos, H. Wan, G. C. Hadjipanayis. V. Papaefthymiou, A. Kostikas, and A. Simopoulos. J. Appl. Phy. **72**, 6967 (1993).

[85] M. Kuzminska, N. Carlier. R. Backov. and E. M. Gaigneaux, Appl. Catal., A **505**, 200 (2015).

[86] D. Milivojevic, B. B. Stojic, V. Jokanovic, Z. Jaglicic, D. Makovec, and N. Jovic, J. Alloys Compd. **595**, 153 (2014).

[87] K. Nadeem, L. Ali, I. Gul, S. Rizwan, and M. Mumtaz, J. Non-Cryst. Solids **404**, 72 (2014).

[88] S. Seraj, B. Mirzayi, and A. Nematollahzadeh, Adv. Powder Technol. **25**, 1520 (2014).

[89] M. D. Carvalho, F. Henriques, L. P. Ferreira, M. Godinho, and M. M. Cruz, J. Solid State Chem. **201**, 144 (2013).

[90] N. M. Deraz, and A. Alarifi, Ceram. Int. **38**, 4049 (2012).

[91] K. Nadeem, H. Krenn, W. Sarwar, and M. Mumtaz, Appl. Surf. Sci. **288**, 677 (677).

[92] T. Tuutijärvi, J. Lu, M. Sillanpää, and G. Chen, J. Hazard. Mater. **166**, 1415 (2009).

[93] J. Drbohlavova, R. Hrdy, V. Adam, R. Kizek, O. Schneeweiss, and J. Hubalek, Sensors **9**, 2352 (2009).

[94] L. Zhao, H. Yang, Y. Cui, X. Zhao, and S. Feng, J. Mater. Sci. **42**, 4110 (2007).

[95] S. Zhang, D. Dong, Yu Sui, Z. Liu, H. Wang, Z. Qian, and W. Su, J. Alloys Comp. **415**, 257 (2006).

[96] D. Fiorani, A. M. Testa, F. Lucari, F. D. Orazio, and H. Romero, Physica B **320**, 122 (2002).

[97] Y. L. Zub. "Sol-Gel Methods for Materials Processing", Springer Netherlands (2008).

[98] B. D. Cullity. "Elements of X-Ray Diffraction", Addison-Wesley (1956).

[99] R. S. Khandpur, "Handbook of Biomedical Instrumentation", 3rd edition, McGraw Hill Education. New York (2014).

[100] D. Brandon, and W. D. Kaplan, "Microstructural Characterization of Materials", 2nd edition. John Wiley and Sons (2008).

[101] Applications Bulletin. "Overview of Mechanical Testing Standards", CSM Instruments (2002).

[102] A. Authier, "Dynamical Theory of X-ray Diffraction", Oxford University Press, Oxford (2001).

[103] J. L. Amoros, "The Laue method", Academic Press, London (1975).

[104] http://www.xtal.iqfr.csic.es/Cristalografia/parte_02-en.html

[105] R. E. Dinnebier, "Powder Diffraction: Theory and Practice", Royal Society of Chemistry, Cambridge (2008).

[106] J. S. Blakemore, "Solid State Physics", Press syndicate of the University of Cambridge (1985).

[107] K. Vijayan, A. Mani, C. Balasingh, and A. K. Singh, Scr. Mater. 20, 1767 (1986).

[108] O. Johari, "Scanning Electron Microscopy", SEM, AMF O'Hare, Ill. (1979).

[109] A. A. Christy, and Y. Ozaki, "Modern Fourier Transform Infrared Spectroscopy", Elsevier, Amsterdam (2001).

[110] A. A. Michelson, "Light Waves and Their Uses", University of Chicago Press, Chicago (1903).

[111] Y. leng, "Material characterization", John Wiley & Sons (2008).

[112] C. B. Smith, "Fundamentals of Fourier Transform Infrared Spectroscopy", 2nd edition, CRC Press, Boca Raton, FL (2011).

[113] K. K. Likharev, "Dynamics of Josephson Junctions and Circuits", Gordon and Breach Science Publishers, New York (1986).

[114] https://cathywagnerblog.wordpress.com/tag/faith-healing/

[115] K. P. Thummer, M. C. Chhantbar, K. B. Modi, G. J. Baldha, and H. H. Joshi, J. Mag. Mag. Mater. 23, 280 (2004).

[116] K. Nadeem, H. Krenn, M. Shahid, and I. Letofsky-Papst, Solid State Sci. 19, 27 (2013).

[117] U. Holzwarth, and N. Gibson, Nat. Nanotechnol. 6, 534 (2011).

[118]] G. Blasse, Philips res. Rep. Suppl. 3, 91 (1964).

[119] W. Andra, W. Appel, and H. Danan, "Magnetics", John Wiley & Sons, New York (1990).

[120] L. Néel, A. Geophys. C.N.R.S. 5, 99 (1949).

[121] W. F. Brown, J. Phys. Rev. 130, 1677 (1963).

[122] D. Fiorani, A. M. Testa, F. Lucari, F. D'Orazio, and H. Romero, Phys. B Condens. Matter 320, 122 (2002).

[123] S. Bedanta, and W. Kleemann, J. Phys. D: Appl. Phys. 42, 013001 (2009).

[124] K. Mandal, S. Mitra, and P. A. Kumar, Europhys. Lett. 75, 4 (2006).

[125] K. Nadeem, and H. Krenn, J. Supercond. Nov. Magn. 24, 717 (2011).

[126] B. Martínez, X. Obradors, L. Balcells, A. Rouanet, and C. Monty, Phys. Rev. Lett. 80, 181 (1998).

[127] K. Maaz, A. Mumtaz, S. K. Hasanain, and M. F. Bertino, J. Magn. Magn. Mater. 322, 2199 (2010).

[128] S. Larumbe, J. I. Pérez-Landazábal, J. M. Pastor, and C. Gómez-Polo, J. Appl. Phys. 111, 4306 (2012).

[129] M. Suzuki, S. Fullem, L. Wang, and C. Zhong, Phys Rev B. 79, 024418 (2007).

[130] L. Pavesi, and M. Ceschini, Phys. Rev. B 50, 2047 (1994).

[131] K. Nadeem, W. Zhang, D. Y. Chen, Z. A. Ren, and X. G. Qiu, Nature 5, 10700 (2015).

[132] M. Sasaki, P. E. Jonsson, and H. Takayama, Phys. Rev. B 67, 214422 (2003).